ELECTROMECHANICAL BALLSCREW FORCE EXCITATION SYSTEM: DYNAMIC MODELING AND CONTROL

A THESIS SUBMITTED TO
THE GRADUATE SCHOOL OF NATURAL AND APPLIED SCIENCES
OF
MIDDLE EAST TECHNICAL UNIVERSITY

BY

BURAK DENIZHAN

IN PARTIAL FULFILLMENT OF THE REQUIREMENTS
FOR
THE DEGREE OF MASTER OF SCIENCE
IN
MECHANICAL ENGINEERING

APRIL 2020

Approval of the thesis:

ELECTROMECHANICAL BALLSCREW FORCE EXCITATION SYSTEM: DYNAMIC MODELING AND CONTROL

submitted by **BURAK DENIZHAN** in partial fulfillment of the requirements for the degree of **Master of Science in Mechanical Engineering Department, Middle East Technical University** by,

Prof. Dr. Halil Kalıpçılar
Dean, Graduate School of **Natural and Applied Sciences** _______________

Prof. Dr. M. A. Sahir Arıkan
Head of Department, **Mechanical Engineering** _______________

Assoc. Prof. Dr. Yiğit Yazıcıoğlu
Supervisor, **Mechanical Engineering, METU** _______________

Examining Committee Members:

Prof. Dr. Ender Ciğeroğlu
Mechanical Engineering, METU _______________

Assoc. Prof. Dr. Yiğit Yazıcıoğlu
Mechanical Engineering, METU _______________

Assoc. Prof. Dr. Afşar Saranlı
Electrical and Electronics Engineering, METU _______________

Assoc. Prof. Dr. Yiğit Taşcıoğlu
Mechanical Engineering, TED University _______________

Assist. Prof. Dr. Ali Emre Turgut
Mechanical Engineering, METU _______________

Date: 29.04.2020

I hereby declare that all information in this document has been obtained and presented in accordance with academic rules and ethical conduct. I also declare that, as required by these rules and conduct, I have fully cited and referenced all material and results that are not original to this work.

Name, Surname: Burak Denizhan

Signature :

ABSTRACT

ELECTROMECHANICAL BALLSCREW FORCE EXCITATION SYSTEM: DYNAMIC MODELING AND CONTROL

Denizhan, Burak
M.S., Department of Mechanical Engineering
Supervisor: Assoc. Prof. Dr. Yiğit Yazıcıoğlu

April 2020, 87 pages

Ball screws are components that are used to convert rotary motion into linear motion with relatively high mechanical efficiency. This property makes them an ideal choice for missile fin actuation systems where the demand for limited volume and high torque exists. Because of the structure of these systems, this high torque demand comes with a high axial force on the ball screw, which consists of a nut, a shaft and balls in between. Especially, on high rotational speeds, the dynamic load capacity of ball screw plays an important role on the overall system performance. Hence, examining this property of the ball screw is critical. Since these application-specific ball screws have short strokes for accelerating the nut or shaft to the desired rotational speed, it is challenging to apply desired load to the nut in this limited period of time. In this study, a test rig is designed to test and verify the dynamic load capacity of ball screws with variable rotational speeds and load factors. Furthermore, mathematical modeling of the test rig is derived and the coefficients of the derived model are estimated through system identification principles by utilizing experimental data. Moreover, a robust force controller acting on the ball screws is synthesized and the mathematical model of the system with uncertainties is analyzed under the effect of the controller in simulation environment and experimentally. Lastly, surplus force caused by the axial movement of the ball screws is decreased through proposed feed-forward controller. The simulation and experimental results show the efficiency of the

designed robust feedback and the proposed feedforward controllers on the system.

Keywords: Ballscrew, Robust Controller, Force Control, Feed Forward Control

ÖZ

ELEKTROMEKANİK BİLYAVİDA KUVVET UYGULAMA SİSTEMİ: DİNAMİK MODELLEME VE DENETİM

Denizhan, Burak
Yüksek Lisans, Makina Mühendisliği Bölümü
Tez Yöneticisi: Doç. Dr. Yiğit Yazıcıoğlu

April 2020, 87 sayfa

Bilyavidalar, dönme hareketini nispeten yüksek mekanik verimlilikle doğrusal harekete dönüştüren bileşenlerdir. Bu özellikleri, bilyavidaları kısıtlı hacim ve yüksek tork gerektiren füze kanatçık tahrik sistemleri için ideal bir seçim haline getirmektedir. Bu mekanizmaların yapısı gereği, belirtilen tork gereksinimi; bir somun, bir mil ve aralarındaki bilyalardan oluşan bilyavida üzerinde eksenel yük olarak ortaya çıkmaktadır. Özellikle yüksek dönme hızlarında, bilyavidaların dinamik yük taşıma kapasiteleri, tüm sistem başarımında önemli bir rol oynar. Bu sebeple, bilyavidaların bu niteliklerinin incelenmesi kritik bir öneme sahiptir. Bahsedilen uygulamaya özel bilyavidalar, somun ya da mili istenilen dönme hızına ulaştırmak için kısa bir kursa sahip olduklarından, bu kısıtlı zamanda istenen yükü somuna uygulamak zorlu olabilmektedir. Bu çalışmada, bilyavidaların dinamik yük taşıma kapasitelerini değişken dönme hızları ve yük faktörleri altında test etmek ve doğrulamak için bir test düzeneği tasarlanmıştır. Çalışmada ayrıca, bu elektromekanik sistemin dinamik modellenmesi yapılmış ve türetilen modeldeki parametrelerin deneysel veriler kullanılarak sistem tanımlama yöntemleri ile kestirimleri yapılmıştır. Buna ek olarak, bilyavidaya etki eden gürbüz bir kuvvet denetimcisi sentezlenmiş ve belirsizlikleri içeren matematiksel model denetleyici etkisi altında deneysel olarak ve benzetim ortamında çözümlenmiştir. Son olarak, bilyavidanın eksenel hareketinden dolayı oluşan fazla kuvvet etkisi, önerilen ileri beslemeli denetleyici ile azaltılmıştır. Benzetim ve deneysel sonuçlar, tasarlanan

gürbüz denetleyici ve önerilen ileri beslemeli denetleyicinin etkinliğini göz önüne sermiştir.

Anahtar Kelimeler: Bilyavida, Gürbüz Denetleyici, Kuvvet Denetimi, İleri Beslemeli Denetim

To my family...

ACKNOWLEDGMENTS

I would like to express my gratitude to my supervisor Assoc. Prof. Dr. Yiğit Yazıcıoğlu for his guidance, support and understanding throughout this work.

I would like to specially thank my colleague Yasin Yeniaydın for his endless help and valuable contributions. I also want to send my thanks to Tuncay Uğurlu Ölçer, Dr. Mete Aydemir, Dr. Bülent Özkan and my head of division Berkay Baykara for giving me the motivation and their helpful criticism. I would like to extend my thanks to Berk Berkan Turgut, Dr. Galip Serdar Tombul, Hamza Kamişli and Dr. Ersin Daş for their support in both technical and moral aspects.

I would like to express my appreciation to TÜBİTAK-SAGE for the facilities and providing the support for the test setup for experimental studies.

I am very grateful to my parents Ayşe Denizhan and Halil Denizhan and my sister Zeynep Ahsen Denizhan for being there for me all the time.

Finally, I would like to send my special thanks to my love Tuğba. She gave me all the motivation, energy and support during this study. I could not finish this work without her help.

TABLE OF CONTENTS

LIST OF TABLES

TABLES

LIST OF FIGURES

FIGURES

LIST OF ABBREVIATIONS

ABBREVIATIONS	
ACDCC	Actuator Command Dynamic Compensation Control
ADRC	Active Disturbance Rejection Controller
BLDC	Brushless Direct Current
CAD	Computer Aided Design
DC	Direct Current
FAS	Fin Actuation System
FES	Force Excitation System
FFT	Fast Fourier Transform
GM	Gain Margin
LFT	Linear Fractional Transformation
LTI	Linear Time Invariant
MIMO	Multi Input Multi Output
PID	Proportional-Integral-Derivative
PM	Phase Margin
RBS	Random Binary Sequence
RMS	Root Mean Square
RP	Robust Performance
RS	Robust Stability
SISO	Single Input Single Output
SSV	Singular Structured Value
SVD	Singular Value Decomposition
VAF	Variance Accounted For

CHAPTER 1

INTRODUCTION

Fin Actuation Systems (FAS) are mechanisms that move the control surfaces of a missile to maintain its trajectory. Since the available space is limited inside missiles, FAS are designed to work with relatively low factor of safety, which means that the subcomponents are selected to operate at boundaries of structural performance most of the time. One of the essential subcomponents of an electromechanical FAS is the ball screw. Ball screw converts the rotary motion into linear motion, or in other words, converting torque into force or vice versa. Because of the aerodynamic effects, an external load is created on the nut of the ball screw and the ball screw should overcome this load while moving. The static load carrying capability of any ball screw can be estimated or tested relatively easy. However, determining the dynamic load carrying capabilities of these custom made ball screws are challenging due to their complex geometry and miniature design. Therefore, a specific test bench is necessary to test the dynamic performance of the ball screw under certain loading conditions. In the scope of this study, a load simulator in the form of an electromechanical test bench is designed to perform the tests of custom made ball screws. These tests will include constant and varying loads that could be encountered during normal operation. The test bench that will simulate these loads includes two BLDC motors, one linear actuator, an elastic element, and other mechanical parts. Because of the mechanical couplings and nonlinear behavior of the elastic element, the system has parametric uncertainties that are hard to be modeled. In order to operate the system within the desired performance limits, a robust controller is synthesized and applied. The robust controller used in this work is an H_∞ controller which is designed and simulated in computer environment, then implemented using a real-time target device.

1.1 Scope of the Thesis

Most of the engineering study starts at the laboratory level. Before any study or prototype transform into a product, they need to be tested under the environmental or operating conditions which a product will encounter during the lifetime. Testing those conditions in the real operating conditions and environmental conditions may become costly. That is why simulators are needed to mimic these conditions at the laboratory level. By doing that, any kind of failure is prevented before the product being tested in the real environment. In the scope of this thesis, a load simulator is going to be designed. A load simulator is simply a device, which is capable of creating the constant or varying loads, which the test subject will encounter during its operation.

1.2 Literature Research

In this section, various Force Excitation Systems (FES), i.e., load simulators, are analyzed. Simulating a load is a force control problem in the end. Consequently, force control systems are also investigated. In this study, an electromechanically actuated force excitation system is designed. However, independent from the actuation mechanism, the concept of a load simulator is the same for all. Thus, in this section, different FES are examined in terms of design, modeling, and control.

It is common to see the interaction between the actuator and the load being as stiff as possible [1]. This has many advantages, such as increasing the bandwidth of the system and reducing instability. As much as high stiffness has advantages, low stiffness introduces a significant number of advantages as well. [1] and [2] introduced series elasticity by inserting a passive elastic element between the actuator and the load. By adding this elasticity, the stiffness is reduced. The advantage of reducing the stiffness is firstly increasing the force resolution, which makes the force control a lot easier. However, there is a trade-off between high stiffness and low stiffness. The controllability increases by reducing the stiffness; nevertheless, the bandwidth of the system also reduces simultaneously. Thus, choosing the elastic element between load and actuator is crucial in this case. Another benefit of using series elasticity is converting the force control problem into a position control problem [1], assuming that the introduced elasticity is linear and known.

In [3], an electrohydraulic load simulator that applies an aerodynamic load to the rudder of an aerobat is designed. The system is an electronic-hydraulic system which outputs desired torque by utilizing μ synthesis to eliminate the conservatism of H_∞ controllers. In addition, robust performance and robust stability are analyzed. In the experiments, the designed robust controller is compared with a classical controller in terms of desired reference torque tracking under different disturbances, and the results show the superiority of the robust controller.

[4] designs and analyzes an electric load simulator with and without a spring beam through a feedforward controller based on invariance theory. The simulator consists of a DC motor for applying required torque, spring beam, position sensors to measure rotation angle of the spring beam, torque sensor, and a simulated rudder. Moreover, the mathematical model of the system is derived, and the stability of the system based on the stiffness of the spring beam is analyzed. Experimental results with the spring beam and feedforward controller show improved reference tracking.

In [5], an electric load system of a flight simulator is analyzed, and the mathematical model of the designed system is derived. The system generates required load torque via a DC motor. In addition, closed-loop torque control for simulating aerodynamic disturbances applied to an aircraft is carried out in a simulation environment. Furthermore, a feedforward controller is designed to eliminate disturbances arising from the position of tested rudder in the testbed. Lastly, simulation results show that closed-loop control, together with feedforward control, decreases steady-state error.

[6] puts forward an electrical aerodynamic loading system and proposes a control law based on sliding mode to test flight actuation systems. The loading system is basically comprised of a Brushless Direct Current (BLDC) motor and its driving unit for the loading and torque sensor. Moreover, there exist a direct mechanical connection between the loading motor and the flight actuation mechanism. This leads to the utilization of the BLDC motors with high torque constant. Furthermore, the desired torque is provided with adaptive fuzzy sliding mode control law. The control law consists of three independent terms: one is for reference torque tracking, one is for

friction compensation estimated through fuzzy logic, and the other one is for compensation of disturbance effect due to rotation of tested flight actuation mechanism. Lastly, the stability of the closed-loop system is analyzed in the sense of Lyapunov, and simulation results of reference torque tracking are given.

[7] proposes a nonlinear adaptive robust controller that compensates for Coulomb friction and ensures a stable parameter adaptation for an electro-hydraulic system designed for hardware-in-the-loop simulation for flight actuation mechanism. In addition, a nonlinear mathematical model of the system is derived. Lastly, the proposed control method is compared with conventional PID control. Simulation and experimental results confirm the superiority of the suggested method in terms of reference tracking under disturbances caused by the operation of the tested actuator mechanism.

In [8], the controller design of an electro-hydraulic load simulator based on PID and velocity synchronized feedforward control for realizing hardware-in-the-loop testing of actuators is proposed. In addition, the nonlinear mathematical model of the system is derived. This work exploits the velocity and acceleration of the tested actuators for feedforward control design. Simulation and experimental results indicate that the proposed feedforward control, together with the PID control, achieves better reference tracking than the conventional feedforward control, which uses the position of the tested actuators together with the PID control.

Force control on an electro-hydraulic actuator is realized under the disturbance of a moving system in [9]. In the control scheme, velocity and disturbance force are measured as feedbacks, and analysis of relative robustness and noise sensitivity are carried out in frequency domain. A comparative study between conventional proportional control and the proposed control scheme shows the superiority of the proposed method in terms of reference tracking under the disturbances due to the moving system.

In [10], a dynamic load simulator simulating aerodynamic hinge moment applied to an aircraft actuation system is designed to test the actuation system on the ground. To design the load simulator, [10] first derives a linear mathematical model of the dynamic load simulator and analyzes the frequency response of the load simulator. Then, a robust Quantitative Feedback Theory force controller taking into account uncertainties of the load simulator is designed to generate the required hinge moment.

In [11], an electrical load simulator is designed and controlled for the performance testing of actuators. For the design of the load simulator, a rigid connection between the load motor and tested actuator through a torque sensor is formed. This work first derives the mathematical model of the system by considering the tested actuator as a disturbance torque and afterward analyzes the disturbance torque to compensate for it. Subsequently, an adaptive controller taking the parameter uncertainty and the disturbance torque into account is designed through the position command of the tested actuator. In the experiments, the proposed controller is compared with the PI controller in terms of reference torque tracking under the sinusoidal disturbance of the tested actuator.

[12] designs H_∞ based controller of a load simulator for the electric steering gear. For the controller design, additional torque due to rotation of the electric steering gear is analyzed in the frequency domain and considered as a feedforward controller for torque control of the load simulator. For evaluation, the H_∞ and feedforward controller together are compared with the PI controller in terms of reference tracking under disturbances arising from the movement of the tested electric steering gear in the simulation environment. [13] focuses on eliminating surplus torque on an electric motor loading simulator by exploiting Active Disturbance Rejection Controller (ADRC). This study first derives the mathematical model of the system by combining voltage and torque balance equations of a DC motor. Moreover, the system is disturbed via angle position of the loaded motor. Next, ADRC is designed by considering nonlinearities and uncertainties of the system. In addition, parameter tuning of the ADRC is explained. The designed controller is compared with a conventional PID controller with a feedforward controller in terms of suppressing surplus torque and reference torque tracking in the simulation environment.

In [14], an adaptive robust controller is proposed for electrical loading simulator, which simulates aerodynamic torque to test flight actuators on the ground. This work takes account of a rigid connection between loading and loaded systems through a torque sensor and derives a linear mathematical model with bounded parameter uncertainties of the system. Furthermore, extra torque due to acceleration and speed differences between loading and loaded systems and disturbance torque due to parameter variations are estimated. In the last step, an adaptive robust controller, which takes account of the estimated extra torque and disturbance torque, is designed, and stability of the system is analyzed in the sense of Lyapunov. In the simulation environment, torque tracking response is observed by considering parametric uncertainties.

[15] designs a mixed sensitivity H_∞ controller for an electric load simulator for testing actuation systems of an aircraft on the ground. The optimization problem of mixed sensitivity H_∞ controller for sensitivity function, complementary sensitivity function, and the output of the controller in the frequency domain is constituted through predefined weighting functions. After solving the optimization problem, the obtained controller is tested in relation to reference tracking under the disturbance of the loaded system due to movement of it in simulation and experimental environments.

[16] designs an electrohydraulic load simulator to test flight actuation systems on the ground. The system is mainly composed of an actuator, torque sensor, and a hydraulic motor. The hydraulic motor and the actuator are connected through the torque sensor. This research work first derives the mathematical model of the system and surplus torque, which is dependent on the movement of the actuator and the loading motor. After that, PID controller with Actuator Command Dynamic Compensation Control (ACDCC), which utilizes actuator command signal for suppressing the surplus torque, is proposed for reference torque tracking. The proposed method is analyzed in terms of reference torque tracking under disturbances in different frequencies.

In [17], a hydraulic workbench is designed for applying force to primary flight actuators on the ground. The workbench is mainly based on a hydraulic load actuator, load cell, lever arm, and a flight actuator. In this work, uncertainties of hydraulic parameters are investigated, and the plant model is analyzed in frequency domain. Furthermore, robust force control based on Loop-Shaping approach is designed, and optimal bandwidth is determined through robustness analysis. Lastly, closed-loop performance is analyzed in frequency and time domains.

[18] proposes the Fuzzy-PID force controller for a hydraulic load simulator basically composed of hydraulic motor, pressure sensor, load cell, and additionally a controlled disturbance. In this work, the controller is based on fuzzy interference via predeter-

mined membership functions for the P, I, D parameters to avoid deriving a mathematical model of the hydraulic system due to nonlinearities and parameter variations of the system arising from flow-pressure relation and fluctuation pressure, respectively. In experiments, conventional PID is compared with the Fuzzy-PID controller under the controlled disturbances in terms of reference tracking.

In [19], a Fuzzy-PID force controller for a hydraulic load simulator is designed. The load simulator mainly consists of a piston pump, an AC motor, and a control circuit. In order to test the simulator under disturbances, another similar hydraulic circuit is utilized for generating disturbances, and the two hydraulic circuits are connected through a spring, and feedback is provided with a load cell. In this work, fuzzy interference is preferred due to challenges of modeling the hydraulic circuit, and P, I and D parameters are specified through the predetermined membership functions. For experiments, the proposed controller is compared with conventional PID under sinusoidal and white noise disturbances in terms of the step response.

[20] theoretically analyzes and experimentally verifies surplus torque due to tested actuator in an electrohydraulic system where loading and tested electrohydraulic actuators are connected through a torque sensor and a spring. This research concludes that the velocity of the tested actuator is the main factor of the surplus torque.

[21] analyzes gear backlash effects in an electric load system. To do that, [21] first derives a nonlinear model, including gear backlash and friction in the system as a deadband. Then, the analysis of characteristics of the deadband is carried out. Additionally, an inverse compensation method is proposed by adding an offset to the control signal determined by the size of the deadband. Lastly, the proposed compensation method is verified in simulation environment by analyzing output torque.

In [22], a single neuron PID controller is designed for redundant force suppression for an electrohydraulic system. In this research, the schematic of the system is composed of an electrohydraulic load simulator, tested booster, and a force sensor. A rigid connection between the load simulator and the booster is provided with the force sensor. This work designs the single neuron PID, which tunes P, I and D parameters with a predetermined learning rate to compensate for the redundant force caused by the booster movement. At the last step, the proposed compensation technique is compared with traditional feedforward compensation techniques in simulation environments.

In [23], a nonlinear adaptive robust controller is designed for an electrohydraulic load simulator whose schematic is composed of spring, damper, position sensor, torque sensor, loading hydraulic motor, and tested actuator. This work first derives nonlinear state equations. Then, extended state observer for unmeasured states and force controller taking into account transient and steady-state performance by the help of Lyapunov are designed. Lastly, transient and steady-state behavior of closed-loop systems is analyzed in the simulation environment.

1.3 The Outline of the Thesis

In this thesis, the design, modeling, and control of a force excitation system are discussed. In Chapter 1, the literature is reviewed, and similar systems are investigated. In Chapter 2 the mathematical background, which is needed to comprehend the thesis work, is presented. Then in Chapter 3, the designed system is introduced, modeled, and the experimental identification is made. In Chapter 4, a robust controller is designed for the given system, and the stability of the system is investigated. Furthermore, in Chapter 5, with the designed controller, the simulations are made, and the experimental results are collected in real-time application. Finally, in Chapter 6 the results are discussed.

CHAPTER 2

BACKGROUND

2.1 Field

A field is defined as a set F together with two mappings called addition and multiplication [24]. These mappings can be shown respectively as:

$$\begin{aligned} \oplus &: F \times F \to F \\ \odot &: F \times F \to F \end{aligned} \tag{2.1}$$

The properties of addition can be listed as following:

1. Commutativity:
$$a \oplus b = b \oplus a \to \forall a, b \in F \tag{2.2}$$
2. Associativity:
$$a \oplus (b \oplus c) = (a \oplus b) \oplus c \to \forall a, b, c \in F \tag{2.3}$$
3. Additive identity: An element, defined as O_F exists such that,
$$a \oplus O_F = a \to \forall a \in F \tag{2.4}$$
4. Additive inverse: An element, defined as $-a$ exists, for each $a \in F$ such that,
$$a \oplus (-a) = O_F \to \forall a \in F \tag{2.5}$$

For multiplication:

1. Commutativity:

$$a \odot b = b \odot a \rightarrow \forall a, b \in F \tag{2.6}$$

2. Associativity:

$$a \odot (b \odot c) = (a \odot b) \odot c \rightarrow \forall a, b, c \in F \tag{2.7}$$

3. Multiplicative identity: An element, defined as 1_F exists such that,

$$a \odot 1_F = a \rightarrow \forall a \in F \tag{2.8}$$

4. Multiplicative inverse: An element, defined as a^{-1} exists, for each $a \neq O_f$ such that,

$$a \odot (a^{-1}) = 1_F \rightarrow \forall a \in F \tag{2.9}$$

Also both addition and multiplication operations satisfy:

$$a \odot (b \oplus c) = (a \odot b) \oplus (a \odot c) \rightarrow \forall a, b, c \in F \tag{2.10}$$

2.2 Vector Space

A linear space V is defined as a set whose elements are denoted as vectors associated with a field F, whose elements are indicated as scalars and includes both addition $\oplus_v$ and scalar multiplication $\odot_v$ operations [24].

$$\begin{aligned} \oplus_v &: V \times V \rightarrow V \\ \odot_v &: F \times V \rightarrow V \end{aligned} \tag{2.11}$$

The properties of addition can be listed as following:

1. Commutativity:

$$x \oplus_v y = y \oplus_v x \rightarrow \forall x, y \in V \tag{2.12}$$

2. Associativity:

$$x \oplus_v (y \oplus_v z) = (x \oplus_v y) \oplus_v z \rightarrow \forall x, y, z \in V \tag{2.13}$$

3. Additive identity: A vector, defined as O_v exists such that,

$$x \oplus_v O_v = x \rightarrow \forall x \in V \tag{2.14}$$

4. Additive inverse: An element, defined as $-x$ exists, for each $x \in V$ such that,

$$x \oplus_v (-x) = O_v \rightarrow \forall x \in V \tag{2.15}$$

For scalar multiplication, the following properties could be indicated:

1. Property 1

$$a \odot_v (b \odot_v x) = (a \odot_f b) \odot_v x \rightarrow \forall x \in V, \forall a, b \in F \tag{2.16}$$

2. Property 2

$$a \odot_v (x \oplus_v y) = (a \odot_v x) \oplus_v (a \odot_v y) \rightarrow \forall x, y \in V, \forall a \in F \tag{2.17}$$

3. Property 3

$$(a \oplus_F b) \odot_v x = (a \odot_v x) \oplus_v (b \odot_v x) \rightarrow \forall x \in V, \forall a, b \in F \tag{2.18}$$

4. Remembering that the multiplicative identity is 1_F,

$$1_F \odot x = x \rightarrow \forall x \in V \tag{2.19}$$

2.3 Normed Spaces

Let (V, F) be a vector space where V is a linear space and F is a field associated with the linear space V. A norm on V is a function

$$\|.\| : V \rightarrow \mathbb{R} \geq 0 \tag{2.20}$$

satisfying the following properties [25]:

- $\|v\| \geq 0 \quad \forall v \in V$
  $\|v\| = 0 \Leftrightarrow v = 0_v$ where 0_v is a vector whose elements are all zero.

- $\|av\| = |a| \, \|v\| \quad \forall a \in \mathbb{R}, \;\; \forall v \in V$

The triplet $(V, F, \|.\|)$ are called a normed space. Remarks:

- Norm defines a distance between two vectors, v_1 and $v_2 \in V$ with the expression $\|v_1 - v_2\|$.
- Let $V \in \mathbb{R}^2$, $F \in \mathbb{R}$. Then norms can be generalized into what we called as L_p-norms:
  $\|v\|_p = (|v_1|^p + |v_2|^p + ... + |v_n|^p)^{1/p} \quad \forall v = [v_1 \;\; v_2 \;\; ...v_n]^T \in V$
  Here, $[v_1 \;\; v_2 \;\; ...v_n]^T$ is the transpose of $[v_1 \;\; v_2 \;\; ...v_n]$.

2.4 Orthonormal Vectors

The vectors v_1,$v_2 \in V$ are said to be orthonormal if [26]:

$$\|v_1\|_2 = 1, \|v_2\|_2 = 1 \;\; and \;\; v_1 \cdot v_2 = 0 \tag{2.21}$$

The set of vectors, $\{v_1 \;\; v_2 \;\; ...v_n\}$, are said to be mutually orthonormal if [26]:

$$\begin{gathered} \|v_i\|_2 = 1, \;\; i = 1, 2, ..., n \\ v_i \cdot v_j = 0, \quad \forall i \neq j \end{gathered} \tag{2.22}$$

Here, $v_i \cdot v_j = 0$ are the dot product of the vectors v_i and v_j.

2.5 Unitary Matrices

A square, complex matrix (U) is said to be unitary matrix, if its columns and rows consist of mutually orthonormal vectors [26]. Then, a unitary matrix has the following properties:

$$\begin{aligned} U^*U &= I \\ |U| &= 1 \\ U^* &= U^{-1} \end{aligned} \tag{2.23}$$

Here, $|U|$ is the matrix determinant and U^* is the complex conjugate transpose of U.

2.6 Singular Value Decomposition

Let A be an $m \times n$ complex matrix, then A can be written via Singular Value Decomposition (SVD) as [27]:

$$A = UDV^* \tag{2.24}$$

Here, U, D and V are $m \times m$, $m \times n$ and $n \times n$ matrices, respectively. Whereas U and V are unitary matrices, D is a diagonal matrix containing the nonnegative singular values (σ_s) of A.

Let's consider that $m > n$, then we have:

$$U = [u_1 \;\; u_2 \;\; ...u_m]$$

$$D = \begin{bmatrix} \sigma_1 & 0 & \cdots & 0 \\ 0 & \sigma_2 & \cdots & 0 \\ \vdots & \vdots & \ddots & \vdots \\ 0 & 0 & \cdots & \sigma_n \\ \vdots & \vdots & \cdots & \vdots \\ 0 & 0 & 0 & 0 \end{bmatrix} \tag{2.25}$$

$$V = [v_1 \;\; v_2 \;\; ...v_n]$$

with the convention that $\sigma_1 > \sigma_2 > \cdots > \sigma_n$, where $u_1, u_2 \ldots u_m$ and $v_1, v_2 \ldots v_n$ are the columns of U and V, respectively.

Remark: Let's consider that A as a system, then the largest output of the system in the sense of L_2-norm is the largest singular value, σ_1, and the input that generates the largest output is the vector, v_1, corresponding to the largest singular value.

2.7 L_∞ Space

L_∞ is a Banach space, which is a normed vector space which is complete, of matrix or scalar-valued functions (F) which are bounded with norm given in eqn. 2.26 as

$$\|F\|_\infty = \underset{\omega\in\Re}{sup}\bar{\sigma}(F(j\omega)) \tag{2.26}$$

2.8 H_∞ Space

H_∞ is a subspace of L_∞ and it contains functions which are analytic and do not contain open right half poles. The H_∞ norm is given in eqn. 2.27 as

$$\|F\|_\infty = \underset{Re(s)>0}{sup}\ \bar{\sigma}(F(s)) = \underset{\omega\in\Re}{sup}\bar{\sigma}(F(j\omega)) \tag{2.27}$$

2.9 Linear Fractional Transformation

Linear Fractional Transformation (LFT) is a mathematical tool to model the structural and unstructured uncertainties [28]. If we define a generalized plant such that in Figure 2.1, w is denoted as the exogenous input, u is the control signal, z is the performance output and y is the measured variables.

If the generalized plant $P(s)$ is grouped according to the signal types and written in the partitioned matrix form:

$$P(s) = \begin{bmatrix} P_{11} & P_{12} \\ P_{21} & P_{22} \end{bmatrix} \tag{2.28}$$

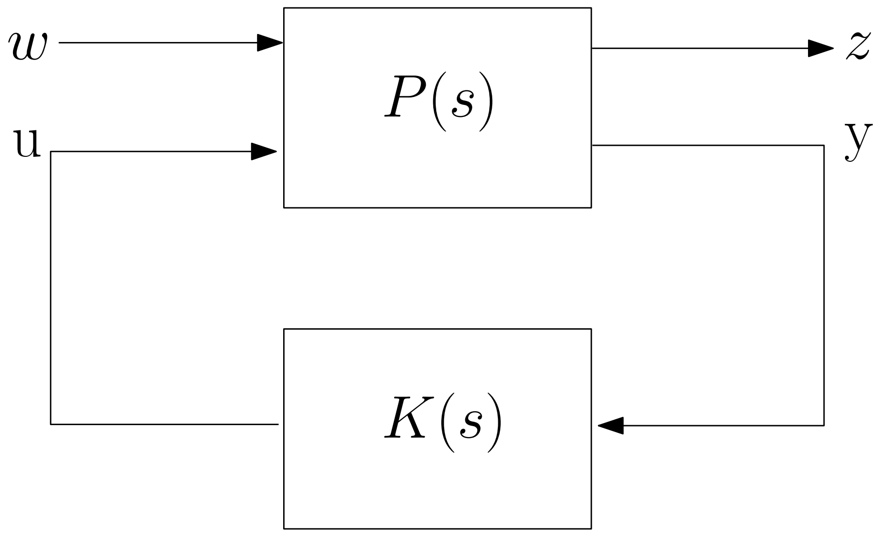

Figure 2.1: Generalized Plant with controller $K(s)$

Then the following expressions could be written:

$$
\begin{aligned}
z &= P_{11}w + P_{12}u \\
y &= P_{21}w + P_{22}u
\end{aligned} \tag{2.29}
$$

Also reminding that:

$$u = K.y \tag{2.30}$$

Substituting 2.30 into 2.29 to eliminate u and y and isolating z yields:

$$z = \left[P_{11} + P_{12}K(I - P_{22}K)^{-1}P_{21}\right] w \tag{2.31}$$

The following expression in 2.31:

$$F_l(P, K) = \left[P_{11} + P_{12}K(I - P_{22}K)^{-1}P_{21}\right] \tag{2.32}$$

is called the Lower Linear Fractional Transformation of P with K.

Similarly, for the most general case, adding uncertainty Δ to the system yields as in Figure 2.2.

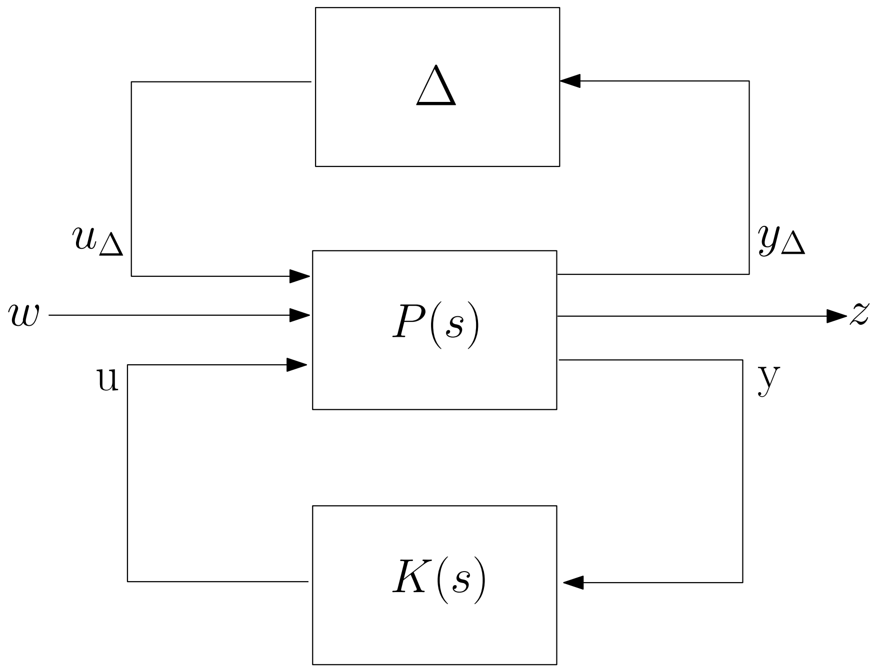

Figure 2.2: Generalized Plant with controller and Uncertainty

If the Lower LFT of P with K is found and named as $N = F_l(P, K)$, the remaining system would look like as in Figure 2.3 and the relation is given as:

$$z = F_u(N, \Delta)w \tag{2.33}$$

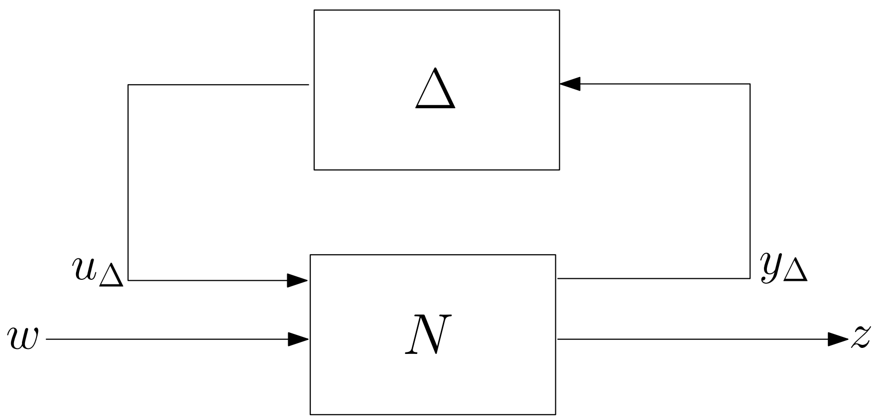

Figure 2.3: Generalized Plant with Uncertainty

This time, Upper Linear Fractional Transformation of N with Δ is given as:

$$F_u(N, \Delta) = \left[N_{22} + N_{21}\Delta(I - N_{11}\Delta)^{-1}N_{12}\right] \tag{2.34}$$

2.10 Small Gain Theorem

For stable blocks of M and Δ, the closed loop system shown in Figure 2.4 is also stable if the following condition is true [29]:

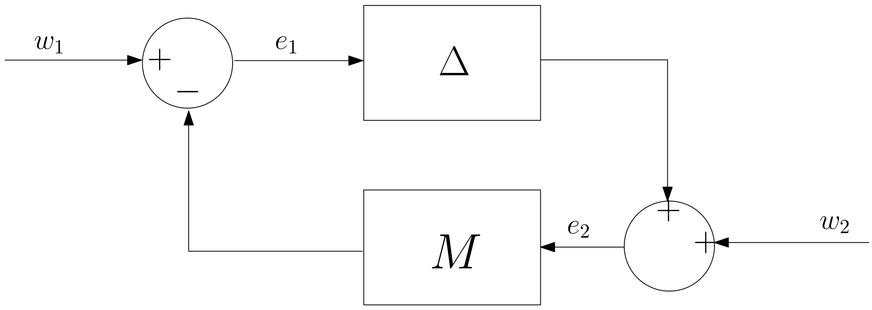

Figure 2.4: The closed loop system with stable blocks

$$\|\Delta\|_\infty \|M\|_\infty < 1 \tag{2.35}$$

We know that $\|\Delta\|_\infty \leq 1$, then $\|M\|_\infty < 1$ is true. However, this could be conservative because each value of $\|\Delta\|_\infty$ and $\|M\|_\infty$ in 2.35 might have peaks at different frequencies. Since, 2.35 is the sufficient condition and infinity norms of systems have submultiplicative property, the overall closed loop system may still be stable even if 2.35 is not satisfied.

Then, let us define the Δ block as:

$$\|\Delta\|_\infty \leq \frac{1}{\gamma} \quad \gamma > 0 \tag{2.36}$$

Then the closed loop system is internally stable if:

$$\|M\|_\infty < \gamma \tag{2.37}$$

2.11 Bode Plot

For a linear time invariant (LTI) system, the Bode plot is used to show frequency response of the system across the entire spectrum [30]. For LTI systems, operations that could be used with the input signal are limited with:

- Multiplication by a constant
- Differentiation
- Integration
- Addition

These are important because, for an LTI system, if a harmonic input is given such that:

$$A\sin(a\omega) \rightarrow G(s) \rightarrow B\sin(a\omega + \phi) \tag{2.38}$$

the frequency of the output is the same, while the amplitude and phase of the signal can change. To demonstrate this amplitude and phase shift of the signal on the whole frequency range, two separate graphs are used known as Bode plots as in Figure 2.5

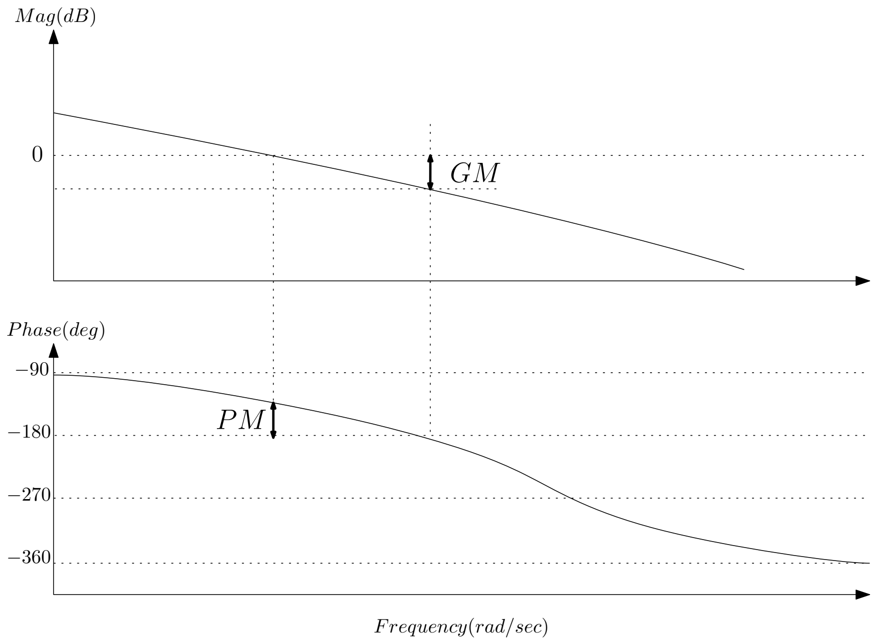

Figure 2.5: A sample Bode plot

Bode plots illustrate steady state frequency response of systems and the illustrated response is composed of amplitude ratio and the phase shift as given in Figure 2.5. For the steady state behavior, steady state phase shift and amplitude ratio of a transfer function can be calculated simply by setting:

$$s = j\omega \tag{2.39}$$

Another important property that could be visually seen on a Bode plot is gain and phase margins of a system, alternatively called as stability margins.

The *gain margin* of a system could be defined as the total variation of the gain to make the system marginally stable.

Similarly, the *phase margin* is defined as how much of the phase can be changed to make the system marginally stable.

These margins could be shown on the Bode plot of a stable transfer function as in Figure 2.5. The gain margin is calculated where the phase of the loop gain crosses -180 degrees. Similarly, the phase margin is determined where the gain of the system crosses 0 dB line, i.e. $|G(j\omega)| = 1$.

2.12 Nyquist Plot

For an LTI system, similar to the Bode plot, another way of demonstrating the gain and phase of a system is Nyquist plot [31]. While two plots are needed for showing the gain and phase margins in Bode plots, these two margins could be shown in a Nyquist plot together as in Figure 2.6.

The gain and phase margins can visually be seen on a Nyquist plot. Wherever the $G(j\omega)H(j\omega)$ crosses the negative real axis of the Nyquist plot (i.e. phase crossover frequency) and call this point as G_{pc}, then the gain margin is:

$$\text{GM} = \frac{1}{G_{\text{pc}}} \tag{2.40}$$

That also means, how much the gain could be increased in order not cross -1 on the negative real axis.

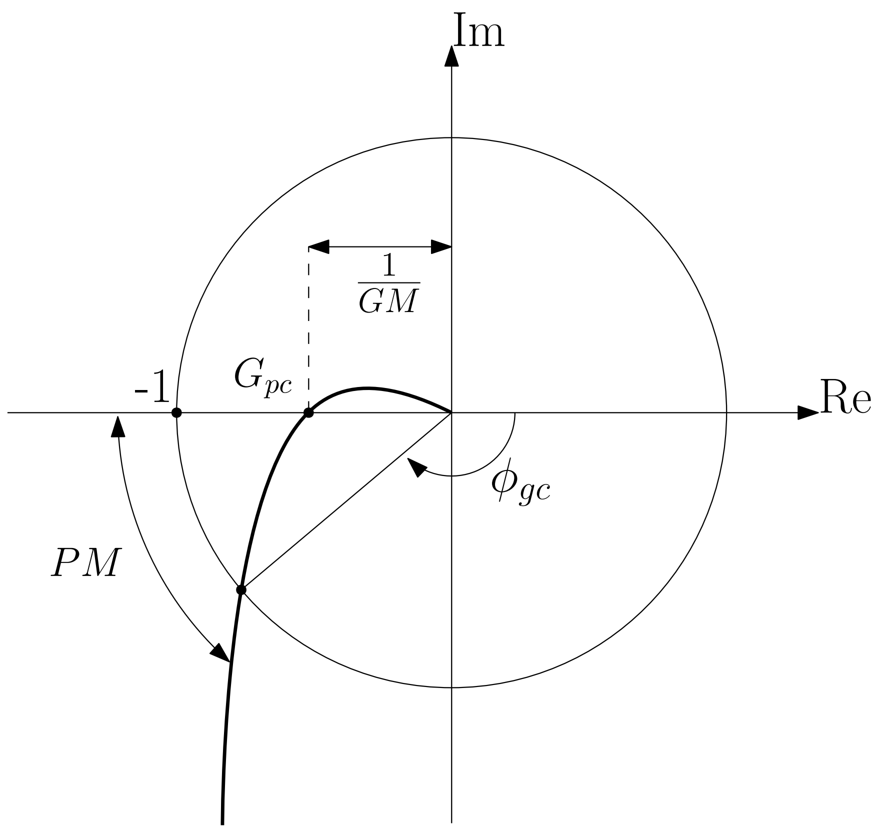

Figure 2.6: Nyquist Plot

Similarly, wherever the $G(j\omega)H(j\omega)$ crosses the unit circle on the Nyquist plot (i.e. gain crossover frequency) and calling the angle of this point on the unit circle as ϕ_{gc}, the phase margin is found as while the sign of the counterclockwise rotation is considered as positive:

$$PM = 180^\circ + \phi_{gc} \tag{2.41}$$

CHAPTER 3

SYSTEM DESIGN, MODELING AND IDENTIFICATION

3.1 Design of the System

3.1.1 Determination of Loading Conditions of Ball Screw

The necessity of designing such a test bench is based on the need to test the ball screw of a FAS at the subcomponent level. Thus, the requirements of the test bench to be designed will arise from the loading conditions of the FAS and, consequently, the ball screw.

The electromechanical FAS covered in this thesis has an inverted slider-crank mechanism. Then, one can show the schematic diagrams of the system as given in Figure 3.1 [32].

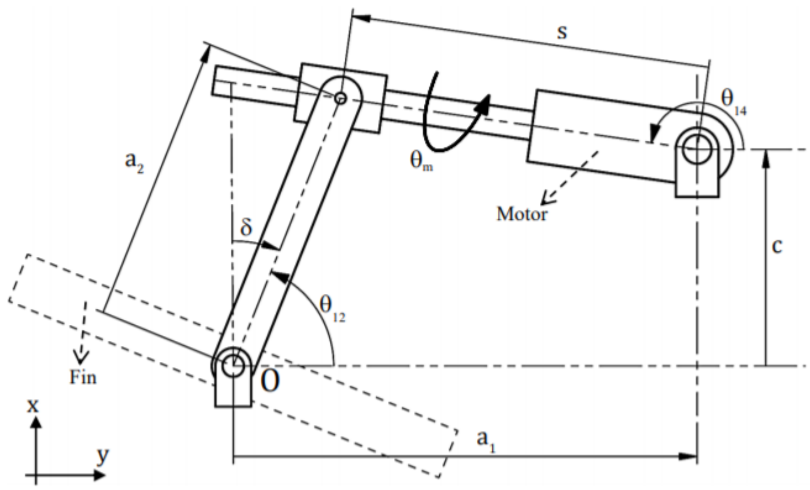

Figure 3.1: The FAS as an inverted slider crank mechanism

In order to find the necessary testing conditions, both the position and load analysis of the system are needed. By using the position analysis, the maximum stroke and the maximum linear velocity of the ball screw can be found. Then, by using the load analysis, maximum axial force transmitted from the fin to the nut through moment arm due to the maximum hinge moment can be found. Identifying those will give the necessary testing conditions for the test bench.

3.1.2 The requirements of the test bench

The test bench should be constructed in order to test the ball screws to meet the following requirements:

- While the test subject ball screw reaches a linear velocity of 70 mm/s, at least 1000 N shall be applied to the nut of the ball screw.
- The force command shall be adjustable.
- The maximum force tracking error (response to the step disturbance) in the existence of disturbance of maximum 1 Hz (position control system operating condition) shall be ± 150 N.
- The bandwidth of the force excitation system should be at least 10 Hz with an amplitude of 100 N.
- The maximum steady state error shall be 20 N.

3.1.3 Description of the Test Rig

The test bench used in this work has two actuators. One actuator is used to rotate the shaft of the tested ball screw. The other actuator is going to be used to impart the necessary load to the nut to simulate the flight loads. In the scope of this work, only the mechanism simulating the flight loads is considered.

As seen in Figure 3.2, the mechanism (Position Control Part) is driven by BLDC Motor 1 is connected to a chuck via a shaft and couplings. The chuck is used to test ball screws with different shaft diameters varying from 4 mm to 25 mm. Self-aligning is also possible with the use of this arrangement.

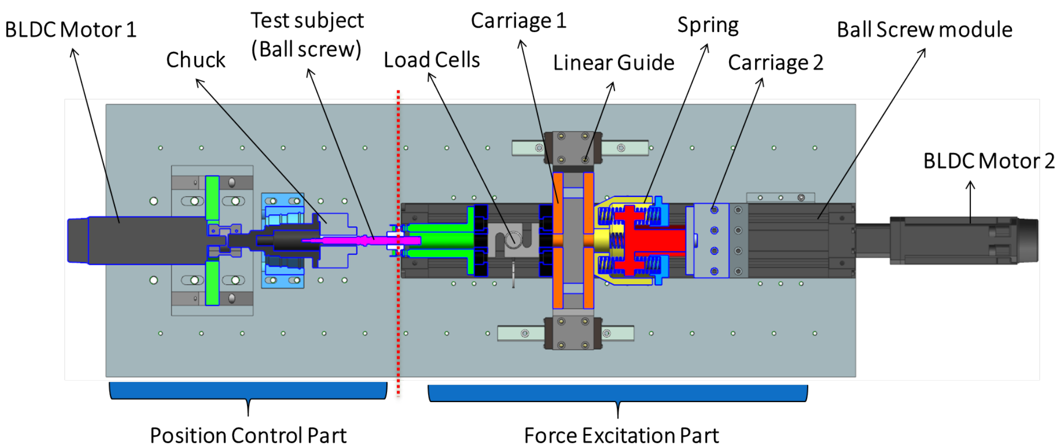

Figure 3.2: The schematic view of the test rig

In Figure 3.2, the mechanism (Force Excitation Part), which is actuated by BLDC Motor 2, simulating the flight loads on the tested ball screw. BLDC Motor 2 is connected to a ball screw module which drives Carriage 2. Carriage 2 is coupled to Carriage 1 with a spring, which allows the test bench to work as a series elastic actuator. Carriage 1 is guided by two profile rail bearings. Finally, Carriage 1 is in series with two tandem load cells, which are connected to the nut of the tested ball screw for applying the load. Also, the CAD model of the test rig is shown is Figure 3.3.

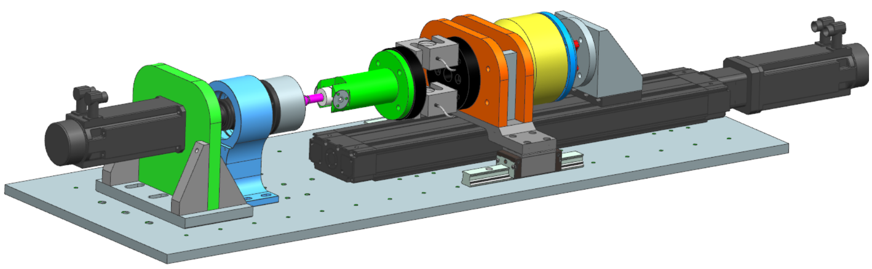

Figure 3.3: The CAD model of the test rig

In this test bench, a particular axial load is applied to the nut of the ball screw, which can move as desired. It is noted that this study does not include the working principles of motion mechanism of the ball screw.

3.1.4 Design of the Test Rig

In this section, the design of the proposed system will be explained in detail. As mentioned in the previous sections, this system consists of two BLDC electric motors, chuck, rail guides, springs, and auxiliary mechanical parts. This system could be divided into two parts as:

- Force Excitation Part
- Position Control Part

The position control part is responsible for actuating the tested ball screw with the predefined position reference under the effect of force disturbance. On the other hand, the force excitation part applies the desired force while the position control part drives the ball screw. As mentioned in Section 3.1.2, the position control part drives the tested ball screw with the given specifications in Table 3.1.

Table 3.1: Specifications for the position control part

Max. Speed	70 mm/s
Lead of the Ball Screw	4 mm
Stroke of the Ball Screw	40 mm

3.1.4.1 Design of the Force Excitation Part

By considering the requirements of the test bench, among the alternatives of hydraulic, pneumatic or electromechanical actuators, an electromechanical system is preferred and a brushless direct current (BLDC) motor is selected to drive the system.

Using a BLDC actuator has following advantages over hydraulic, pneumatic and brushed DC motors [33] [34]:

- More compact and easy to install

- Less noise and more robust system (there could be losses in the hydraulic pipes)
- The maintenance is much easier (less pollution, no need to change the hydraulic fluid, no brushes for commutation)
- More efficient than a hydraulic setup or a brushed DC motor.
- Allowing more sophisticated control methods over pneumatic and hydraulic systems
- Commutation is performed electronically by hall sensors placed on the stator of the motor. This electronic commutation increases the controllability of the system.
- Better speed/torque characteristics. Possibility of operating at all speed levels with the rated torque. Even more for a limited time.
- Comparative dynamic response due to the low rotor inertia
- Suitable for moderate loads.

An in runner BLDC motor consists of three main elements as in Figure 3.4 [34]:

- Rotor (magnets placed on top of it),
- Stator (where the windings take place),
- Hall sensors and the electrical circuit for resistances

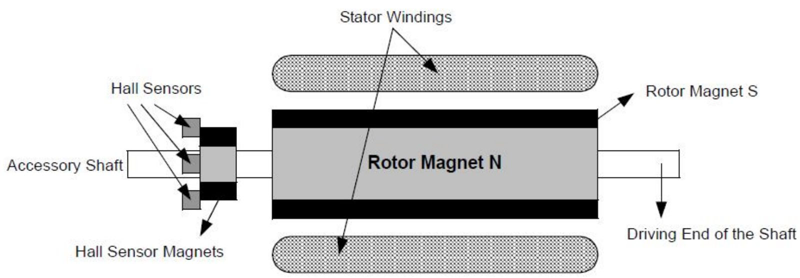

Figure 3.4: BLDC electric motor components

A DC electric motor can be expressed mathematically as in eqn. 3.1.

$$V = E + IR + L\frac{dI}{dt} \tag{3.1}$$

Where V the applied armature voltage, while E is the Electromotor Force which is motion dependent. R and L are the internal resistance and the inductance of the motor caused by the windings, respectively. Also, I is the current flowing through the coils.

Here, one can see the equivalent motor circuit as in Figure 3.5 [35].

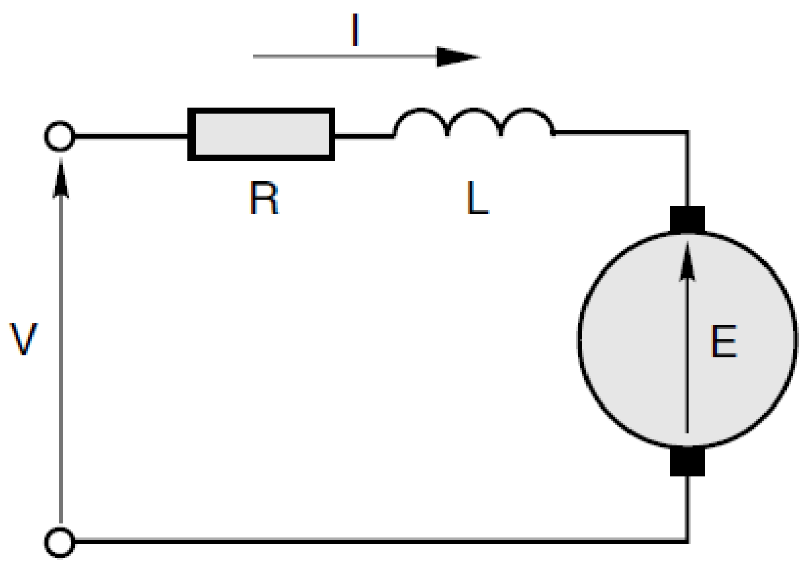

Figure 3.5: Equivalent motor circuit

Assuming that voltage supply is enough and ignoring the higheer order internal dynamics, the mechanical output of the motor can be represented as in eqn. 3.2.

$$T = k_t I \tag{3.2}$$

Where T is the output torque, and k_t is the motor torque constant.

For an electric motor in motion, assuming the components are rigid and ignoring the nonlinear dynamics, this mechanical output is equal to:

$$T = k_t I = J\ddot{\theta} + B\ddot{\theta} \tag{3.3}$$

Where J is the total inertia, B is the viscous damping, and θ is the angular position of the rotor.

3.2 Mathematical Modeling of the System

In this Section, only the mathematical model of the force excitation part of the test bench is derived in a detailed form. For the modeling and identification purposes, the test rig is decoupled from the elastic element. Furthermore, by doing that, it is possible to model two decoupled parts of the system as rigid bodies, assuming that the only elastic element is the spring in between and it behaves linearly in its operating range.

After the systems are decoupled from the spring, the remaining system is an electromechanical ball screw driven stage. The tested ball screw is mechanically coupled to the BLDC motor via a chuck.

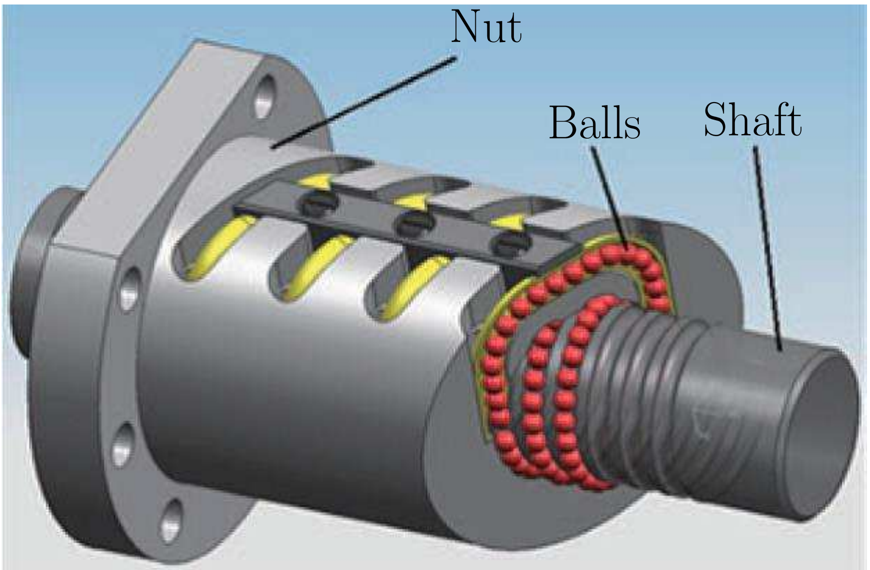

Figure 3.6: Ball screw with an internal recirculation system

A ball screw is an efficient transmission element, which, in general, converts rotation into linear motion. Also, this leads to conversion of torque into force. Ball screws are the same as lead screws in principle. However, ball screws consist of three elements, as in Figure 3.6 [36], which are:

- Screw part
- Nut
- Recirculating balls

Different from lead screws, having balls between the shaft and the nut of the ball screw ensures the motion and the power to be transmitted via rotating balls. This combination provides a significant improvement in friction and dynamic response.

The relation between the angular position of the shaft and the linear position of the ball screw nut is given as [37] :

$$x = \theta \frac{l}{2\pi} \tag{3.4}$$

Where l is the lead of the ball screw. Similar to that, the relationship between the torque and force, assuming that there is no loss due to efficiency, is given as:

$$T = F \frac{l}{2\pi} \tag{3.5}$$

Another important aspect to model in the system is inertia. The total inertia of the system can be found as:

$$J_T = J_s + J_L \tag{3.6}$$

Here, J_T is the total inertia of the system, whereas J_s is the inertia of the screw part and the rotor and J_L is the total reflected inertia of the carriage on the motor shaft. The reflected inertia can be found as follows:

$$J_L = M_L \left(\frac{l}{2\pi} \right)^2 \tag{3.7}$$

Here, M_L can be defined as the total mass of the load driven by the ball screw itself.

For force control, one option is to use position data of two decoupled systems and multiplying this with the known spring constant. However, since this is an indirect solution due to the derivation of force using position data, getting the feedback from the load cell directly will give the most accurate data for force control. Therefore, the states will be selected as the force and the derivative of the force and the equations will be derived to obtain these states.

Based on these definitions, one can write the coupling force between the systems utilizing the spring and both motor positions such that:

$$F = k(x_f - x_p) \tag{3.8}$$

Here x_f and x_p denote the positions of the force excitation and the position control part, respectively. k is the spring constant of the series elastic element. Let us assume that $x_p k$ is unknown and treat it as a disturbance as in [38], then the remaining part is:

$$F = kx_f \tag{3.9}$$

Since x_f is the linear position, using eqn. 3.4, this equation can be rewritten as:

$$F = k\theta_f \frac{l}{2\pi} \tag{3.10}$$

Using the mechanical motor equation defined in eqn. 3.3 and adding the previously ignored external disturbance, the equation on the motor becomes:

$$T = k_t I = J\ddot{\theta} + B\dot{\theta} + T_{ex} \tag{3.11}$$

Since the force is measured and a state, one can obtain the equations explicitly in terms of force. In order to do that, the position variables are substituted using eqn. 3.10, and the equation becomes:

$$k_t I = J\frac{2\pi}{kl}\ddot{F} + B\frac{2\pi}{kl}\dot{F} + T_{ex} \tag{3.12}$$

As a final step, the disturbance T_{ex} should be written in terms of force. Therefore, one should substitute eqn. 3.5 into eqn. 3.12 to obtain:

$$k_t I = J\frac{2\pi}{kl}\ddot{F} + B\frac{2\pi}{kl}\dot{F} + \frac{l}{2\pi}F \tag{3.13}$$

Since it is commonly used in control theory, this expression could be expressed in the state-space model. By denoting:

$$\begin{aligned} x_1 &= F \\ x_2 &= \dot{F} \\ I &= u \end{aligned} \tag{3.14}$$

Then the mathematical model of FES in state-space form is constructed as:

$$\begin{bmatrix} \dot{x_1} \\ \dot{x_2} \end{bmatrix} = \begin{bmatrix} 0 & 1 \\ -\frac{l^2 k}{4\pi^2 J} & \frac{-B}{J} \end{bmatrix} \begin{bmatrix} x_1 \\ x_2 \end{bmatrix} + \begin{bmatrix} 0 \\ \frac{k_t k l}{2\pi J} \end{bmatrix} u$$

$$y = \begin{bmatrix} 1 & 0 \end{bmatrix} \begin{bmatrix} x_1 \\ x_2 \end{bmatrix} \tag{3.15}$$

Here, the state and output matrices could be labeled as such:

$$A = \begin{bmatrix} 0 & 1 \\ -\frac{l^2 k}{4\pi^2 J} & \frac{-B}{J} \end{bmatrix}$$

$$B = \begin{bmatrix} 0 \\ \frac{k_t k l}{2\pi J} \end{bmatrix} \tag{3.16}$$

$$C = \begin{bmatrix} 1 & 0 \end{bmatrix} \begin{bmatrix} x_1 \\ x_2 \end{bmatrix}$$

$$D = 0$$

3.3 System Identification

Here, a model-based controller is going to be used. Therefore, a mathematical model of the dynamic system is needed for the model-based controller. If all the parameters of the system are known, a mathematical model can be obtained theoretically. However, it is not possible to predict all the parameters exactly. The reason for this could be nonlinear, time-dependent or non-deterministic behaviors of friction and electric motor characteristics for the electromechanical system. Thus, these parameters should be experimentally determined. To obtain a system model, the basic procedure of system identification is [39] [40];

1. For a known input, collect the data from the system to be identified
2. Constitute a set of models which would represent the system and choose the best one depending on the structure

3. Then to validate the model with another set of input and output data

This procedure is iterative, and if the model is not sufficient, it should be repeated.

3.3.1 Model Selection

The mathematical model of the system to be identified is found as in eqn. 3.16 in the previous section and only parameters that need to be found are J and B. Normally, the identification should be made by assuming the input is current, and the output is the force. However, due to the noisy output of the load cell, and the necessity to lock the system to produce force makes it hard to identify the system. Therefore, in order to find the J and B values, the spring is disregarded. What we are left with is a ball screw driven stage. Then, the identification is carried out from current to the position of the stage which can be simply expressed by the mechanical motor equation as in eqn. 3.17.

$$k_t I(t) = J\ddot{\theta}(t) + B\ddot{\theta}(t) \tag{3.17}$$

Switching to the frequency domain by applying Laplace transform with zero initial conditions yields:

$$k_t I(s) = J\theta(s)s^2 + B\theta(s)s \tag{3.18}$$

Rearranging the equation to obtain the transfer function for current input and motor position output:

$$\frac{\theta(s)}{I(s)} = \frac{k_t}{Js^2 + Bs} \tag{3.19}$$

Here, k_t,J, and B are the unknown parameters.

For identification purposes, MATLAB System Identification Toolbox is used. There are many options to identify a system; however, simple Process Model Estimation is used to identify the unknown parameters. In MATLAB System Identification Toolbox, the most general process model is defined as:

$$G(s) = \frac{K_p(1 + T_{z1}s)}{(1 + T_{p1}s)} e^{sT_d} \tag{3.20}$$

where K_p is the gain, T_{p1} is the time constant, $(-1/T_{z1})$ is the zero, s is the integrator, and T_d is the delay. The number of time constants, zeros, and integrators can be changed. Since there is no delay, T_d is set to "zero". Also, there are no zeros in eqn. 3.19, that is why, $(1 + T_{z1}s)$ is also omitted. To change eqn. 3.19 into the form of eqn. 3.20, eqn. 3.19 can be rewritten as:

$$G(s) = \frac{\theta(s)}{I(s)} = \frac{k_t/B}{(J/B)s^2 + s} = \frac{k_t/B}{s((J/B)s + 1)} \tag{3.21}$$

Also following parameters are defined as such:

$$\begin{aligned} K_p &= \tfrac{k_t}{B} \\ T_{p1} &= \tfrac{J}{B} \end{aligned} \tag{3.22}$$

then the parameters K_p and T_{p1} could be identified using the following process model:

$$G(s) = \frac{\theta(s)}{I(s)} = \frac{K_p}{s(T_{p1}s + 1)} \tag{3.23}$$

Since the model is known, only two parameters will be identified.

3.3.2 Selection of input

For the identification, selection of the input is another critical criterion. Depending on the application, following signals could be selected:

1. General Purpose Signals, which require no optimization and can excite the system in the selected frequency band with a nearly uniform power spectrum.
2. Optimized Test Signals, which needs iterative ways to build and allows user to set and optimize more properties.
3. Advanced Test Signals, which have particular properties such as suppressing the harmonics or optimizing first and second derivatives of a signal.

Since there are no restrictions on the system in general, a general-purpose signal with a selected frequency band can be used. Different input signals can be used for identifying LTI systems. Some of the most well-known signals can be summed as below:

1. Impulse
2. Step
3. Sine Wave
4. White Noise
5. Random Binary Sequence

Impulse Response identification is simple, but it is mostly for continuous systems. For systems with relatively low sampling rate, it may miss some fast dynamics. Furthermore, in the experimental setups, the impulse may not be appropriate for some systems. Step Response could be a better solution in this case, if the topic is identifying the simple characteristics of a system such as time constant and gain. Sine wave input is also another useful signal, though its importance is mostly seen in frequency response methods. Considering an LTI system, since the response of a sine input is another sine with a different magnitude and phase shift, it can give precise results on the frequency domain. However, these methods either used in time domain or contains a single frequency for identification. Then, the other two inputs, "White Noise" and "RBS" signals can be considered for identification purposes.

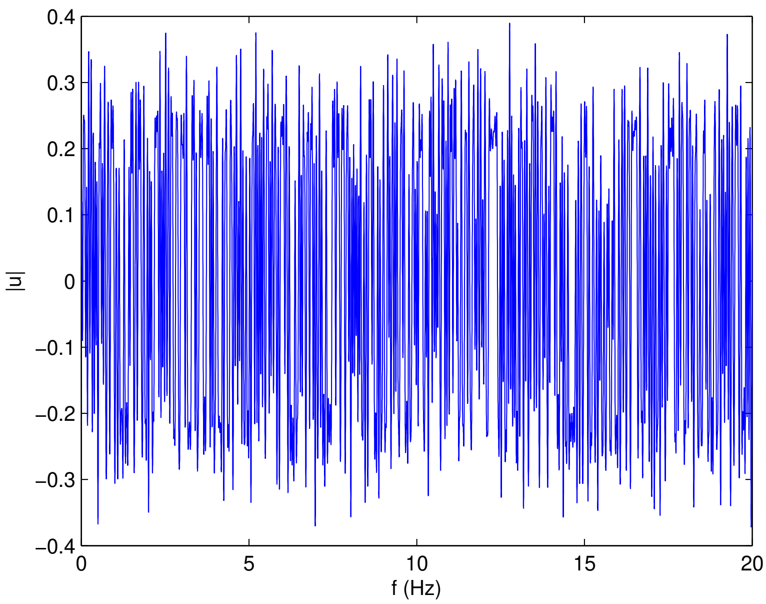

Figure 3.7: Sample white noise

White Noise can be considered as a signal without a time structure. It is a random signal with sequential uncorrelated terms. Also, the white noise has zero mean. Since it has no time structure, it is an excellent way to identify LTI systems. However, using white noise could be inconvenient since the varying amplitudes can be either too large or too small for a known system. This might lead to nonlinear responses of the system to be identified. A sample white noise in time domain can be presented as in 3.7.

On the other hand, a signal with similar characteristics but constrained amplitude, which is called *"Random Binary Sequence"* can be more appropriate for experimental systems. Consequently, Random Binary Signals are used for parameter identification. An example RBS can be seen in Figure 3.8.

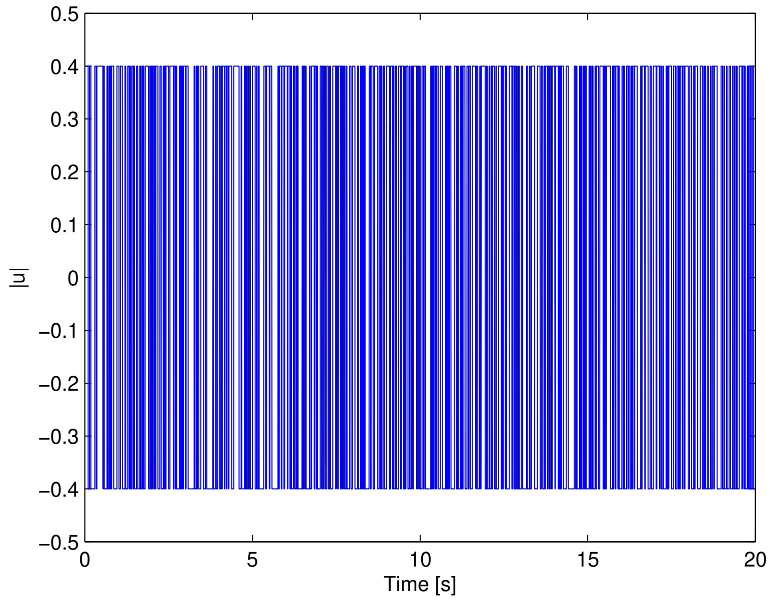

Figure 3.8: Sample Random Binary Sequence

It is also essential to stimulate the system in a relevant frequency range. The loading system in this thesis is expected to work around 10 Hz. Thus, stimulating the system up to at most around 50 Hz will be sufficient to observe the dominant dynamics of the system. Then, a set of RBS signals are used for identification. The RBS input and its FFT, are presented as in Figure 3.9. Here, the current command (RBS input) is directly used rather than using the output of the motor driver as the input of the identification data. Since the working frequency of the motor driver is relatively high, the dynamics of the motor driver is ignored.

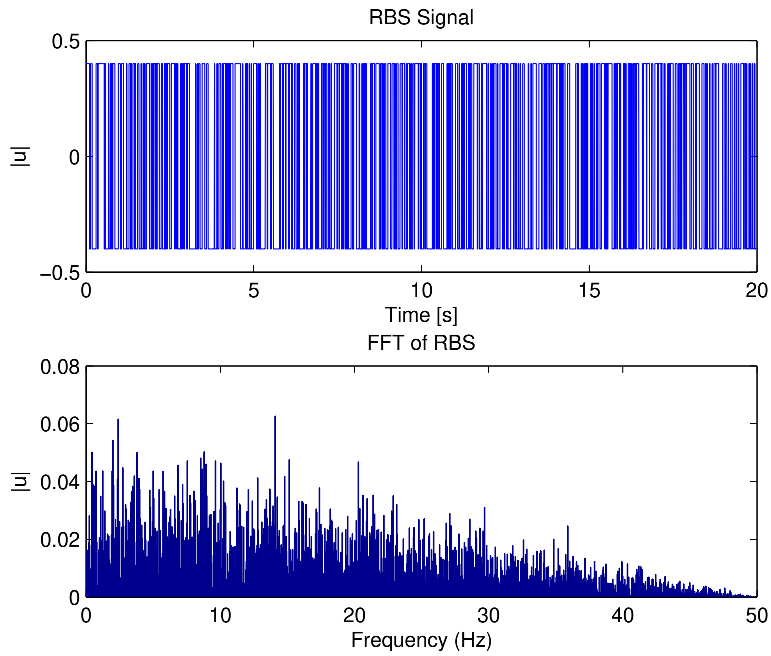

Figure 3.9: Random Binary Sequence input and its FFT

With a few sets of data and using the process model given in eqn. 3.23, the transfer function of the nominal system is identified as:

$$P_1(s) = \frac{\theta(s)}{I(s)} = \frac{750}{s(0.054s + 1)} \tag{3.24}$$

In order to check the "goodness" of the identified data, one can check the Variance Accounted For (VAF) of the real output and the simulated output in response to the same RBS input, using the transfer function obtained in eqn. 3.24. The VAF between two signals is defined as:

$$VAF\% = \left(1 - \frac{var(y - \hat{y})}{var(y)}\right) \times 100 \tag{3.25}$$

Where y is the real output and $\hat{y}$ is the simulated output. The simulated output using eqn. 3.24 and the real output can be seen in Figure 3.10.

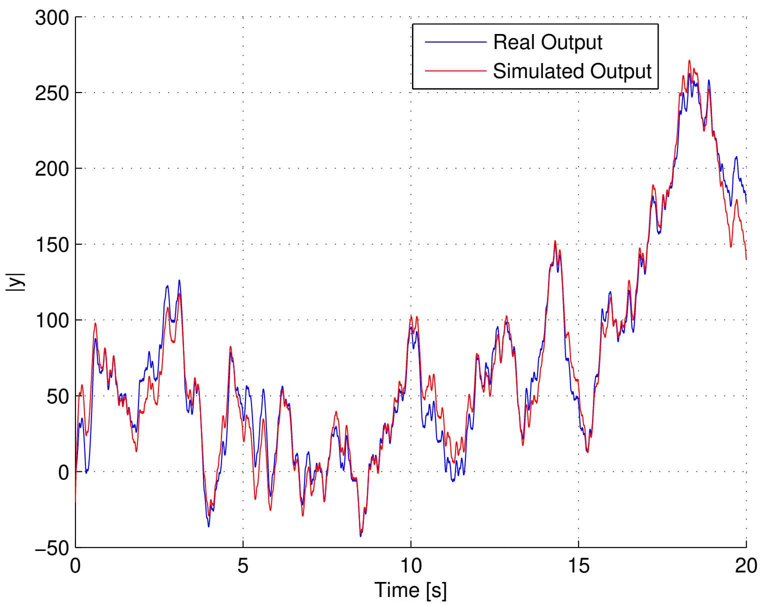

Figure 3.10: The real and simulated outputs for the RBS input

The VAF of these signals are calculated to be 97.3%. The obtained model is verified and validated with other sets of data. Finally, as the nominal model, the transfer function obtained in eqn. 3.24 and using eqn. 3.22, the parameters J and B are calculated since k_t is already known as 1.1 Nm/A from the Electric Motor datasheet as:

$$\begin{gathered} K_p = \frac{k_t}{B} \rightarrow B = 0.0015Nms \\ T_{p1} = \frac{J}{B} \rightarrow J = 7.92 \times 10^{-5} kgm^2 \end{gathered} \tag{3.26}$$

CHAPTER 4

CONTROLLER DESIGN

In this chapter, controller design of the electromechanical test bench which is a single input single output (SISO) system is explained in a detailed way. Hence, the equations throughout the thesis are mostly formulated regarding the SISO systems.

4.1 Internal Stability

All the roots of transfer functions of a closed loop system as shown in Figure 4.1 should be stable to ensure internal stability. In this system, $F(s)$ is a stable transfer function named as prefilter, $K(s)$ is the controller, $P(s)$ is the plant and $H(s)$ is the transfer function of the sensor which provides the feedback.

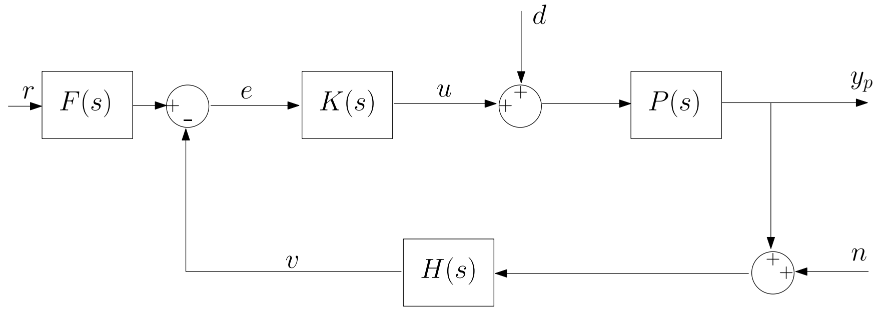

Figure 4.1: A closed loop system

Formally, the internal stability is ensured if

- There do not exist zeros of the system $1 + L$ on the right half plane of the complex plane, where $L = PKH$ is the loop gain. Besides, F is stable.
- There do not exist pole-zero cancellation of the transfer function of L on the

right half-plane of the complex plane.

4.2 Loop Shape

Considering the closed loop system illustrated in Figure 4.2, the transfer functions from all inputs (r, n, d) to performance outputs (e, y_p, u) are given in equations 4.1, 4.2 and 4.3.
It is noted that the term $H(s)$ illustrated in Figure 4.1 is considered as 1 since the output of the system is assumed to be directly utilized.

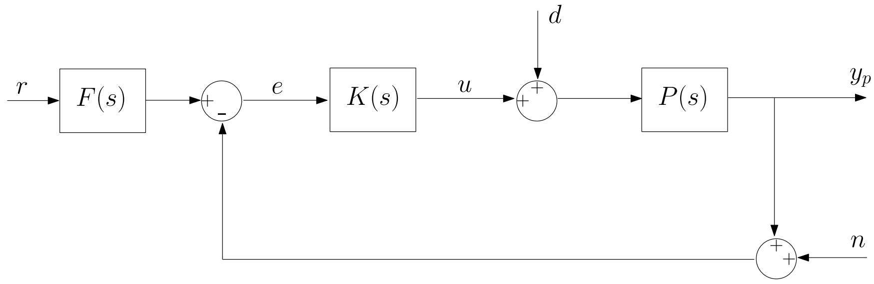

Figure 4.2: A closed loop system without $H(s)$

$$y_p = \frac{PKF}{1+PK}r + \frac{P}{1+PK}d - \frac{PK}{1+PK}n \tag{4.1}$$

$$e = \frac{F}{1+PK}r - \frac{P}{1+PK}d - \frac{1}{1+PK}n \tag{4.2}$$

$$u = \frac{KF}{1+PK}r - \frac{PK}{1+PK}d - \frac{K}{1+PK}n \tag{4.3}$$

The equations are rewritten in the matrix form as

$$\begin{bmatrix} y_p \\ e \\ u \end{bmatrix} = \begin{bmatrix} \frac{PKF}{1+PK} & \frac{P}{1+PK} & -\frac{PK}{1+PK} \\ \frac{F}{1+PK} & -\frac{P}{1+PK} & -\frac{1}{1+PK} \\ \frac{KF}{1+PK} & -\frac{PK}{1+PK} & -\frac{K}{1+PK} \end{bmatrix} \begin{bmatrix} r \\ d \\ n \end{bmatrix} \tag{4.4}$$

Hereby, the terms $sensitivity$ and $complementary\ sensitivity$ are defined in equations 4.5 and 4.6, respectively.

$$S = \frac{1}{1+PK} = \frac{1}{1+L} \tag{4.5}$$

$$T = \frac{PK}{1+PK} = \frac{L}{1+L} \tag{4.6}$$

Using 4.5 and 4.6, equation 4.4 in matrix form can be rewritten as:

$$\begin{bmatrix} y_p \\ e \\ u \end{bmatrix} = \begin{bmatrix} TF & SP & -T \\ SF & -SP & -S \\ SKF & -T & -SK \end{bmatrix} \begin{bmatrix} r \\ d \\ n \end{bmatrix} \tag{4.7}$$

Hence, the relation between the input and output vectors is expressed through S and T.

Further, two additional terms are defined in order to indicate the system behavior, so-called $disturbance$ $(load)$ $sensitivity$ and $noise$ $(control)$ $sensitivity$, respectively.

$$Disturbance\ Sensitivity = PS = \frac{P}{1+PK} \tag{4.8}$$

$$Noise\ Sensitivity = KS = \frac{K}{1+PK} \tag{4.9}$$

The defined transfer functions can be described as follows.

- $Sensitivity$ is a measure of sensitivity of the system to the external inputs.
- $Complementary\ sensitivity$ is the closed loop transfer function (assuming $F = 1$), thus reference tracking and response to sensor noise can be evaluated (Since $S + T = 1$, it is called as $Complementary\ sensitivity$).
- $Load\ sensitivity$ is the effect of disturbance to the output.
- $Noise\ sensitivity$ is the effect of noise to the control input.

Considering the transfer functions, the error between the reference r and the output y_p can be stated as follows by assuming that $F = 1$.

$$\epsilon = y_p - r = -\frac{1}{1+PK}r + \frac{P}{1+PK}d - \frac{PK}{1+PK}n \tag{4.10}$$

Thus, some controller design objectives can be made as follows.

- $\epsilon \to 0$ for precise control. To achieve this, each element on equation 4.10 should go to zero, such that:

$$\epsilon = 0 = -\underbrace{\frac{1}{1+PK}}_{0} r + \underbrace{\frac{P}{1+PK}}_{0} d - \underbrace{\frac{PK}{1+PK}}_{0} n \tag{4.11}$$

  Therefore, higher gain (higher K) helps improving reference tracking and for the disturbance rejection. However, it has an amplifying effect on noise. A lower gain is preferred for noise attenuation.

- Another important aspect is the control signal. Mostly, the control signal is desired to be small since a larger control input means larger energy consumption. Therefore:

$$u = 0 = -\underbrace{\frac{K}{1+PK}}_{\to 0} r - \underbrace{\frac{PK}{1+PK}}_{\to 0} d - \underbrace{\frac{K}{1+PK}}_{\to 0} n \tag{4.12}$$

  Consequently, a lower gain would be preferred for low controller input and keeping the energy lower.

As expressed above, these objectives are conflicting. However, these conflicts can be resolved by applying proper criteria on different frequency ranges. For an electromechanical system, it is generally known that the references and the disturbances are in the relatively low-frequency range, while the noise is in the relatively high-frequency range. Thus, for this purpose, a larger gain would be preferred for low frequencies (in the bandwidth of the system), and a lower gain is favored for higher frequencies (above the bandwidth).

As we have seen, higher gain is desired at some points. However, there is a limit of increasing the gain. Below are the explanation of how the gain increase affects the margins and the stability of the system. As shown in Figure 4.3, increasing the gain reduces both the gain and phase margins of a system, i.e., brings the system closer to the instability. Because of this reason, the gain increase is limited and there is always a trade-off.

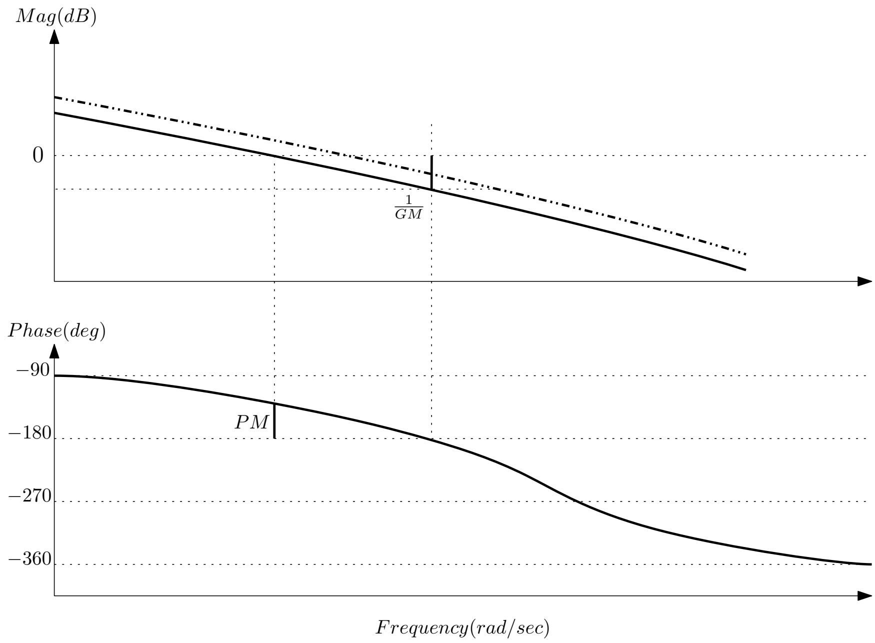

Figure 4.3: Effect of increasing the gain

4.3 H_∞ Norms of SISO Systems

For a given transfer function $G(j\omega)$, the RMS gain (energy) of the transfer function can be stated as the maximum value of its magnitude all over the frequency range shown in Figure 4.4.

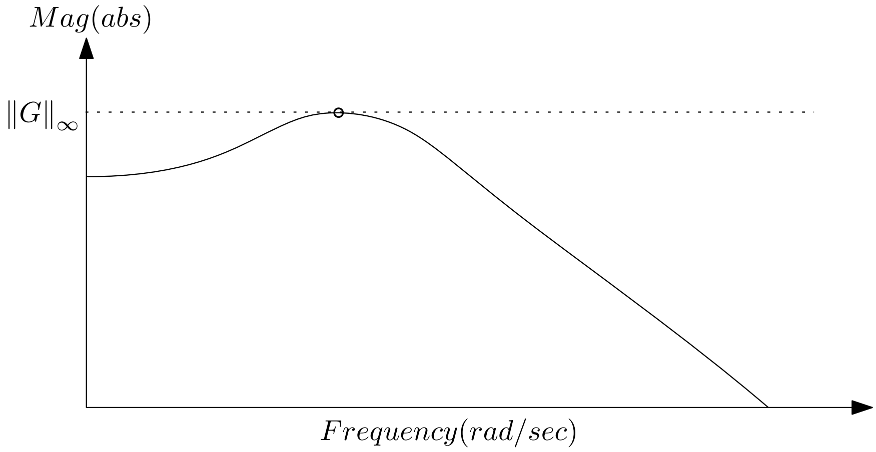

Figure 4.4: RMS gain of a transfer function $G(j\omega)$

The RMS-Gain of G can be given as follows:

$$\|G\|_{rms-gain} = \sup_{\|u\|_{rms} \neq 0} \frac{\|Gu\|_2}{\|u\|_2} \tag{4.13}$$

Also, it can be expressed as:

$$\|G\|_{rms-gain} = \|G\|_\infty = \sup_{\omega} |G(j\omega)| \tag{4.14}$$

4.4 H_∞ Norms of MIMO Systems

For MIMO systems $G(s)$ is a set of transfer functions, which is a matrix. Let us define $H_\infty^{m \times n}$ as the set of $m \times n$ transfer function matrices with elements in H_∞. Then the RMS-gain of a stable MIMO transfer function $G(s)$ can be found as:

$$\|G\|_{rms-gain} = \|G\|_\infty = \sup_{\omega} \bar{\sigma}(G(j\omega)) \tag{4.15}$$

with $\bar{\sigma}$ is the largest singular value.

4.5 H_∞ Norm Controller Design

For H_∞ controller design and analysis, all block diagrams can be "generalized" in order to examine the system in a detailed way. This $generalized\ plant$ can be shown as in Figure 4.5.

Here in Figure 4.5, w are input signals, z are performance output signals, u are control signals and y are measured variables. Also, in this system $P(s)$ contains the weighting functions, which will be explained later on. Assuming that $P(s)$ is a partitioned matrix such that:

$$P(s) = \begin{bmatrix} P_{11} & P_{12} \\ P_{21} & P_{22} \end{bmatrix} \tag{4.16}$$

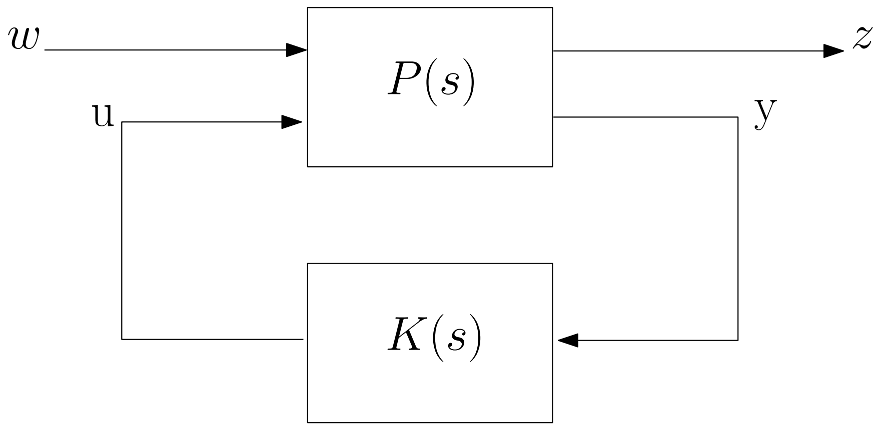

Figure 4.5: Generalized Plant

Then by using the expressions between eqn. 2.31 and eqn. 2.32, the Lower LFT of $P(s)$ with $K(s)$ is computed as

$$F_l(P, K) = \left[P_{11} + P_{12}K(I - P_{22}K)^{-1}P_{21}\right] \tag{4.17}$$

Then the closed-loop transfer function from w to z becomes

$$z = F_l(P, K)w \tag{4.18}$$

The H_∞ controller's objective is to minimize H_∞ norm of $F_l(P, K)$ and the controller is computed by minimizing the H_∞ norms of all transfer functions from w to z.

4.6 H_∞ Norm Controller Architecture

As discussed in the previous section, the H_∞ controller's objective is to find stabilizing controllers which minimize:

$$\|F_l(P, K)\|_\infty = \underset{w(t)\neq 0}{sup}\ \bar{\sigma}(F_l(P, K)(j\omega)) \tag{4.19}$$

The system architecture for the force control problem is given in Figure 4.6.

Here, there are three inputs and three outputs such that

$$\begin{gathered} w_1 = r \quad w_2 = d \quad w_3 = n \\ z_1 = W_1 e \quad z_2 = W_2 u \quad z_3 = W_3 y_p \end{gathered} \tag{4.20}$$

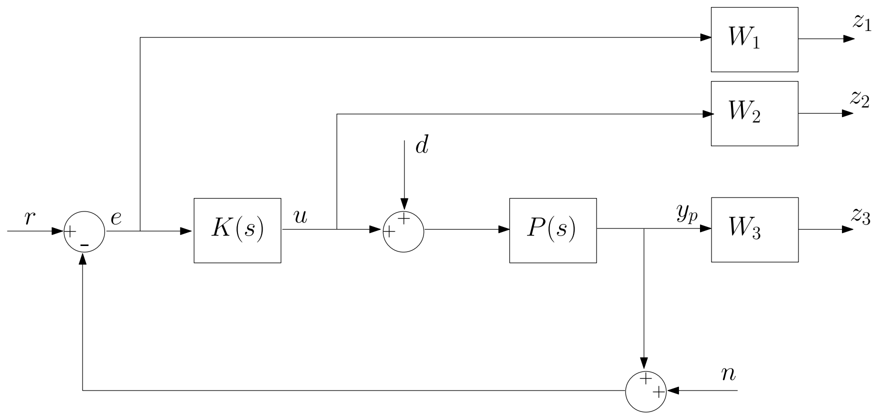

Figure 4.6: System architecture

where W_1, W_2 ,and W_3 are the bounding transfer functions, which are called "$weights$". These $weights$ are utilized for loop-shaping purposes.

In order to "generalize" the plant, the manipulated diagram is shown in Figure 4.7.

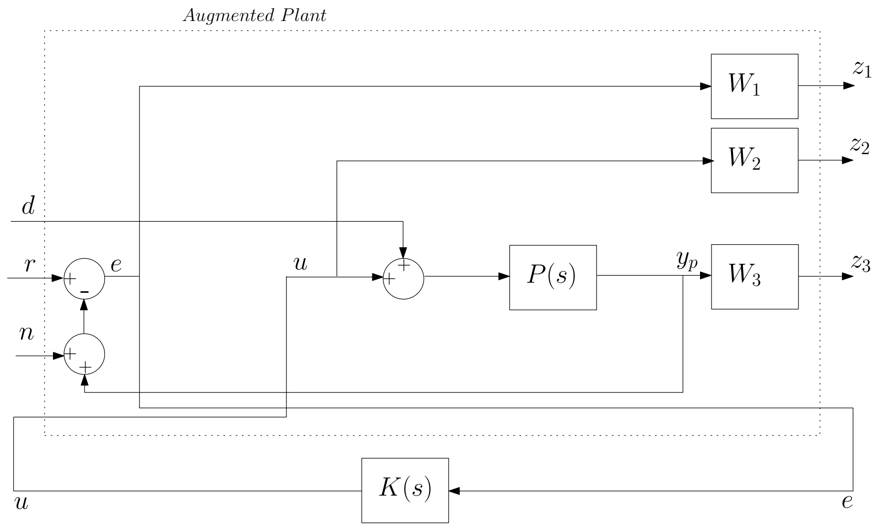

Figure 4.7: Augmented plant

Then by using eqns. 4.1-4.3 and eqn. 4.20, we can write the following relationships, from each w to z.

$$z_1 = \frac{W_1 F}{1+PK} r - \frac{W_1 P}{1+PK} d - \frac{W_1}{1+PK} n \tag{4.21}$$

$$z_2 = \frac{W_2 KF}{1+PK} r - \frac{W_2 PK}{1+PK} d - \frac{W_2 K}{1+PK} n \tag{4.22}$$

$$z_3 = \frac{W_3PKF}{1+PK}r + \frac{W_3P}{1+PK}d - \frac{W_3PK}{1+PK}n \tag{4.23}$$

The equations above is written in the matrix form as

$$\begin{bmatrix} z_1 \\ z_2 \\ z_3 \end{bmatrix} = \begin{bmatrix} \frac{W_1F}{1+PK} & -\frac{W_1P}{1+PK} & -\frac{W_1}{1+PK} \\ \frac{W_2KF}{1+PK} & -\frac{W_2PK}{1+PK} & -\frac{W_2K}{1+PK} \\ \frac{W_3PKF}{1+PK} & \frac{W_3P}{1+PK} & -\frac{W_3PK}{1+PK} \end{bmatrix} \begin{bmatrix} r \\ d \\ n \end{bmatrix} \tag{4.24}$$

In order to uncouple the weightings from each other, two inputs, d and n are dropped down. As can be seen in eqn. 4.24, the weightings are uncoupled from each other but coupled in a way, since they are multiplied with the same transfer function.The new augmented plant is shown in Figure 4.8

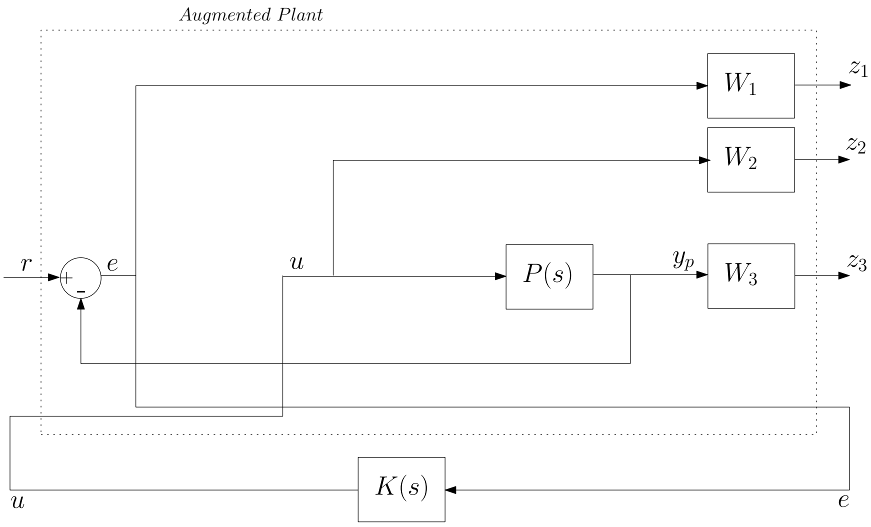

Figure 4.8: Augmented plant with one input and 3 outputs

Then eqns. 4.20 simplifies to

$$\begin{gathered} w_1 = r \\ z_1 = W_1e \quad z_2 = W_2u \quad z_3 = W_3y_p \end{gathered} \tag{4.25}$$

and this problem is also called as *Mixed Sensitivity* problem in control systems.

For a mechanical system, also in force control (our problem), weights are selected with the following methods, assuming mixed sensitivity problem:

- W_1 shapes the error. For a mechanical system, smaller error is desired for low-frequency ranges. However, since the bandwidth of the mechanical system is relatively low, it is desired to be insensitive to the errors in the high-frequency range. Also it is noted that the close loop system is expected to work at around 10 Hz. Since W_1 penalizes the error, W_1 is simply a low pass filter. In this system, W_1 is selected as

$$W_1 = \frac{0.05s^2 + 53.67s + 14400}{s^2 + 15.18s + 57.6} \tag{4.26}$$

And the bode graph of the selected weighting is given in Figure 4.9

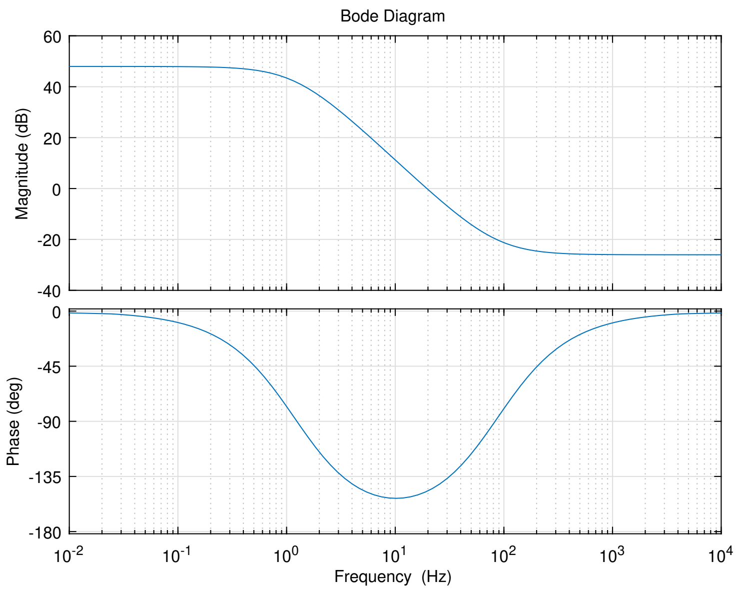

Figure 4.9: Bode plot of W_1

- W_2 shapes the controller input. In this system, the controller input is current. We would want the current to be as high as possible for the low-frequency range. However, in the high-frequency range, the control input should be low, since the high frequency is out of the bandwidth of the system and associated with noise. Since W_2 penalizes the controller input, W_2 is selected as a high pass filter. In this system, W_2 is selected as

$$W_2 = \frac{1.6s + 3}{0.16s + 30} \tag{4.27}$$

The bode graph of the selected weighting is given in Figure 4.10.

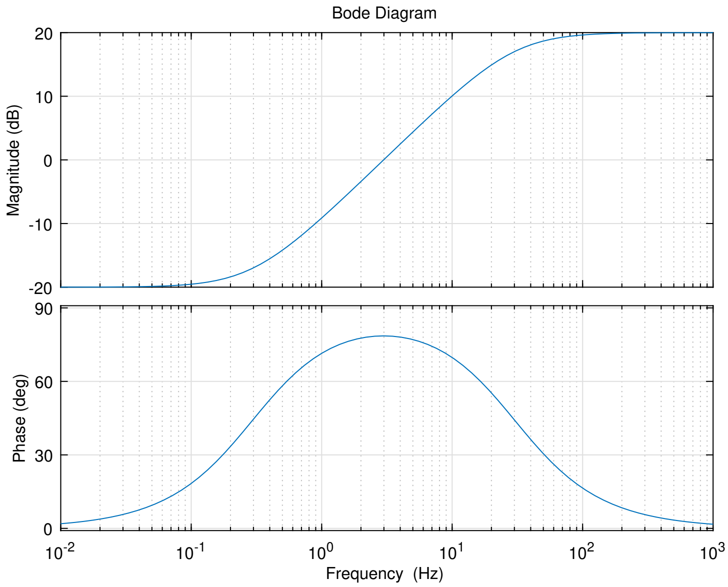

Figure 4.10: Bode plot of W_2

- W_3 shapes the output. For this system, we would want the output to be the same as the reference input for the low-frequency range. Nevertheless, for high frequencies, the output should be low, i.e., the system does not need to give a response on the high-frequency range. Since W_3 penalizes the output, W_3 is selected to be a high pass filter. In this system, W_3 is selected as

$$W_3 = \frac{s + 5000}{0.01s + 15000} \tag{4.28}$$

The bode graph of the selected weighting is given in Figure 4.11.

With the selected weightings, the structure of the augmented plant with the isolated controller as in Figure 4.8 is constructed via MATLAB's $sysic$ function. An H_∞ controller is then synthesized by using MATLAB's built in $hinfsyn$ function.

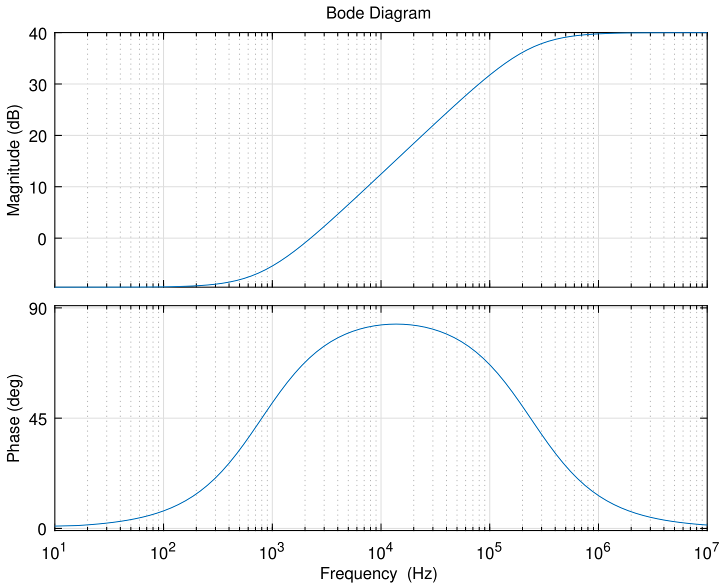

Figure 4.11: Bode plot of W_3

The computed controller in the state space form with A,B,C,D matrices are

$$A = \begin{bmatrix} -15.18 & -7.2 & 0 & -5.575e-11 & 0 & 1.319e-10 \\ 8 & -1.46e-11 & 0 & 8.643e-11 & 0 & -2.045e-10 \\ 21.93 & 270.7 & -188.1 & 0.2301 & -105.7 & -715.2 \\ -4.692e-33 & -1.596e-31 & 0 & -1.5e+06 & 0 & 3.537e+06 \\ 175.5 & 2166 & -4.792 & 1.841 & -864 & -5763 \\ -2.165e-33 & -7.364e-32 & 0 & -1.692e-20 & 64 & 3.999e-20 \end{bmatrix}$$

$$B = \begin{bmatrix} 991.4 - 4.022e - 130 - 5.175e - 211.53e - 24 - 4.637e - 24 \end{bmatrix}^T$$

$$C = \begin{bmatrix} 0.02212 & 0.2731 & -0.0006043 & 0.0002321 & -0.1066 & -0.7215 \end{bmatrix}$$

$$D = 0 \tag{4.29}$$

With the designed controller and the plant, the γ value, which is H_∞ norm of $F_l(P, K)$

is turned out to be 0.9807. Also, the bode plot of the loop gain ($L = GK$) is given in Figure 4.12.

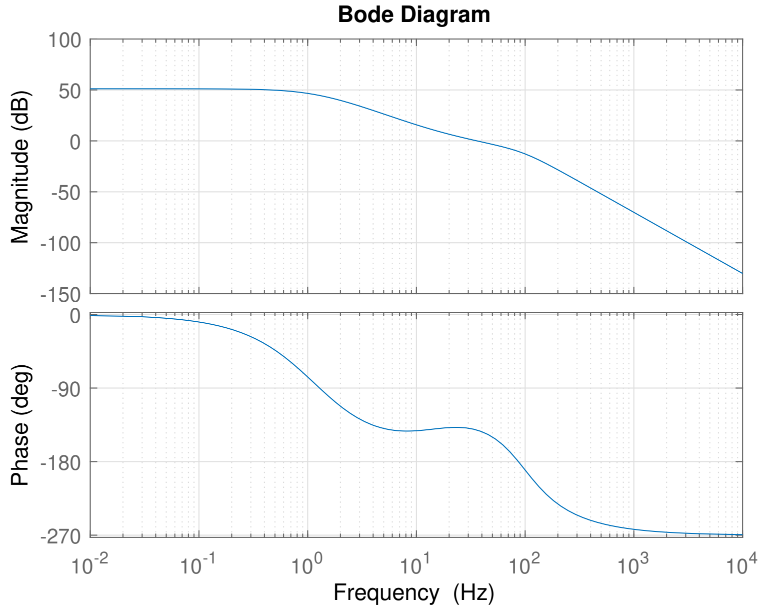

Figure 4.12: Loop gain of the system

The gain and phase margins of the loop gain are given in Figure 4.13.

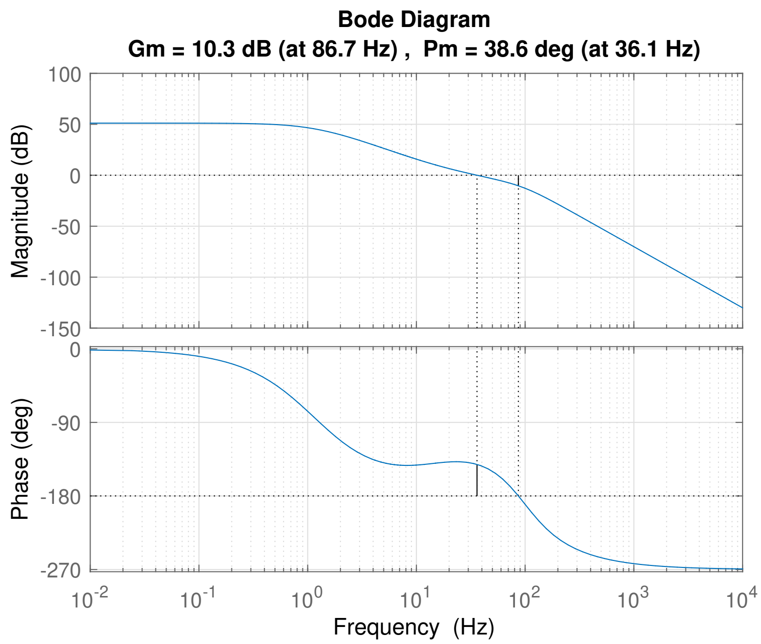

Figure 4.13: Gain and phase margins of the system

As given in Figure 4.13, the gain and phase margins of the nominal loop gain is 10.3 dB and 38.6 degree, respectively. Also the same margins can be observed in the nyquist plot as in Figure 4.14.

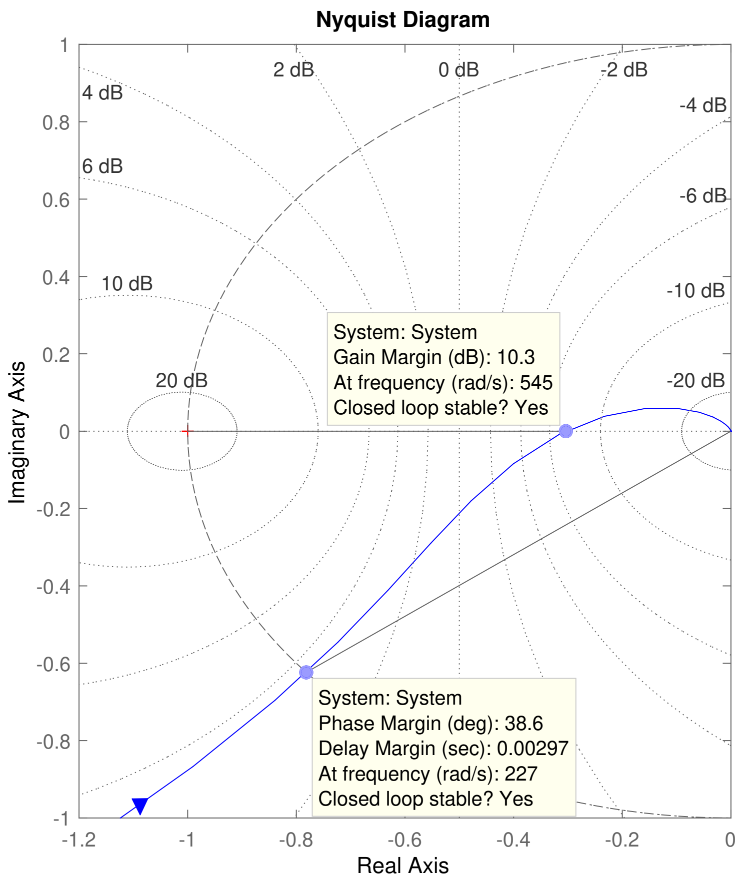

Figure 4.14: Nyquist plot of the system

Since the actuator in the system has a limit, to avoid high increase of derivative of the reference commands, a filter is added on to the system in order to shape the reference signal as in Figure 4.1. This filter approximately corresponds to 20000 N/s and the selected filter is

$$F = \frac{0.01s + 1}{0.025s + 1} \tag{4.30}$$

With the addition of the filter, the closed loop bode plot of the system is given in Figure 4.15. As can be observed from the figure, the closed loop bandwidth of the system corresponds to 11.1 Hz.

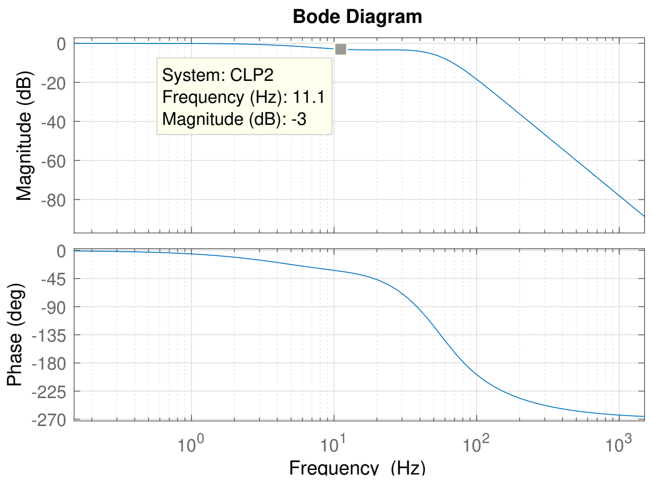

Figure 4.15: Bode plot of the closed loop system

In addition, the bode graphs of each input to each output are plotted. The bode plot of r to e is given in Figure 4.16. As illustrated in Figure 4.16, error is suppressed more for the lower frequencies depending on the bandwidth of the closed loop system.

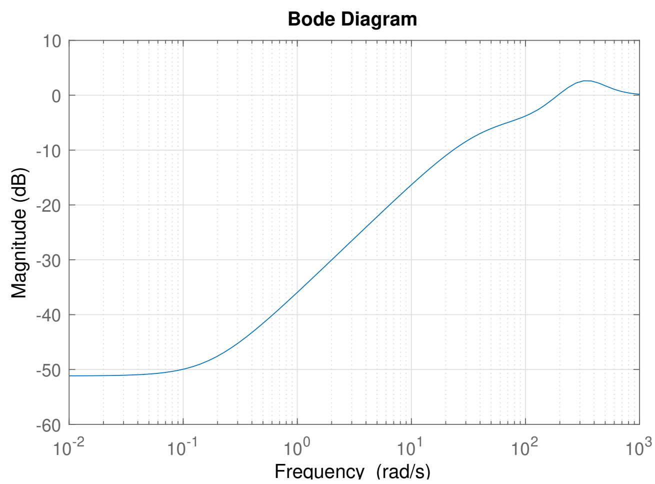

Figure 4.16: The bode plot of r to e

As can be observed from the bode plot of r to u in Figure 4.17, the controller input is comparatively higher in low frequencies to track the reference commands, reject the disturbances in low frequencies better compared to higher frequencies and not to respond to the sensor noise. It is noted that the gain of the transfer function between r to u is small for all frequencies. This arises from the respective units of r $[N]$ and u $[A]$. However, the loop gain is higher in low frequencies.

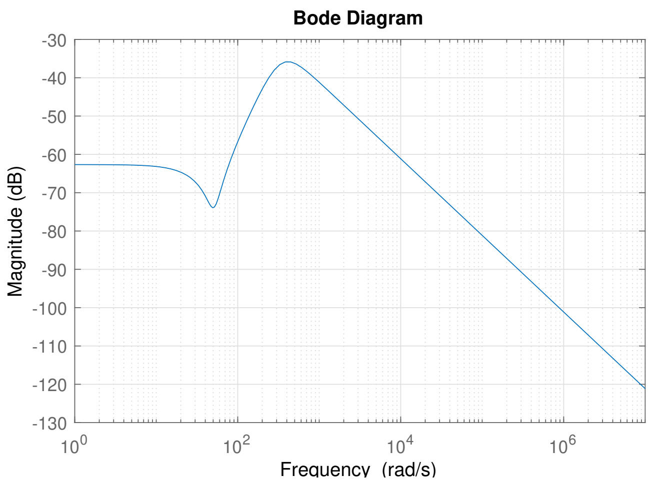

Figure 4.17: The bode plot of r to u

The bode plot of r to y_p is given in Figure 4.18.

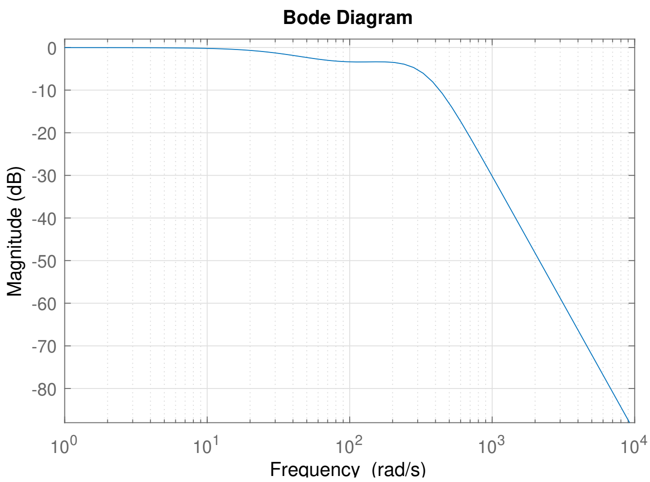

Figure 4.18: The bode plot of r to y_p

As in Figure 4.18, the reference is tracked more closely for the lower frequencies and is not responded for the higher frequencies depending on the bandwidth of the closed loop system.

In the scope of the thesis, it is assumed that the disturbances are effective in low frequencies. As can be interpreted from the bode plot of d to e in Figure 4.19, disturbances are suppressed in low frequencies and the resultant errors are in low level. It is noted that the gain of the transfer function between d to e is higher than 0 dB for all low frequencies. This arises from the respective units of d $[A]$ and e $[N]$.

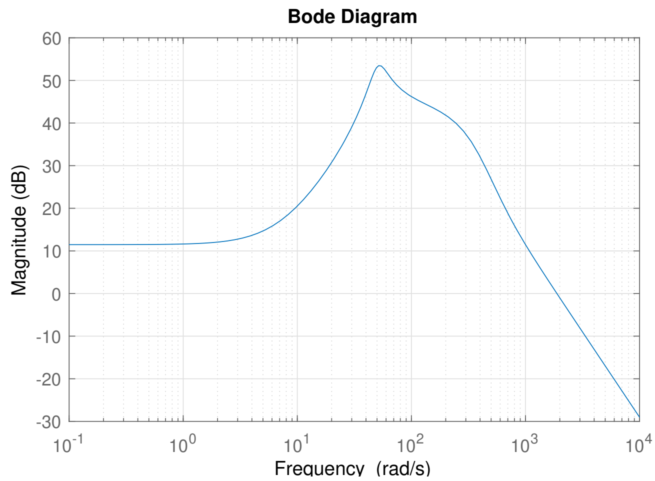

Figure 4.19: The bode plot of d to e

The bode plot of d to u is given in Figure 4.20. To suppress the disturbances which are effective in low frequencies, the required controller gain should be higher in low frequencies as in Figure 4.20.

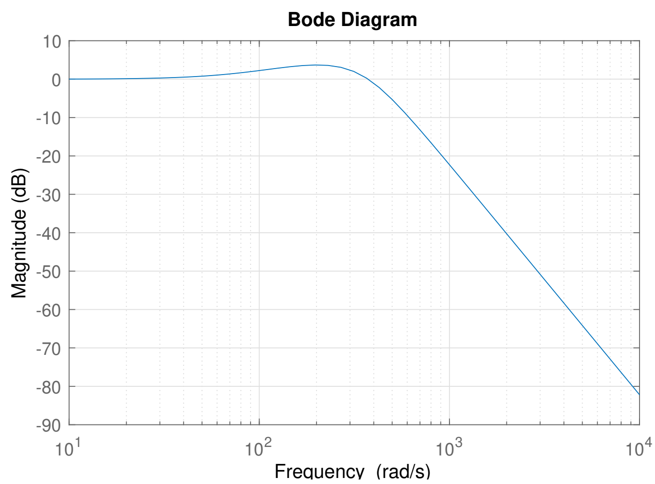

Figure 4.20: The bode plot of d to u

As can be interpreted from the bode plot of d to y_p in Figure 4.21, the efficacy of disturbances on output are small in low frequencies. It is noted that the gain of the transfer function between d to y_p is higher than 0 dB for all low frequencies. This arises from the respective units of d $[A]$ and y_p $[N]$.

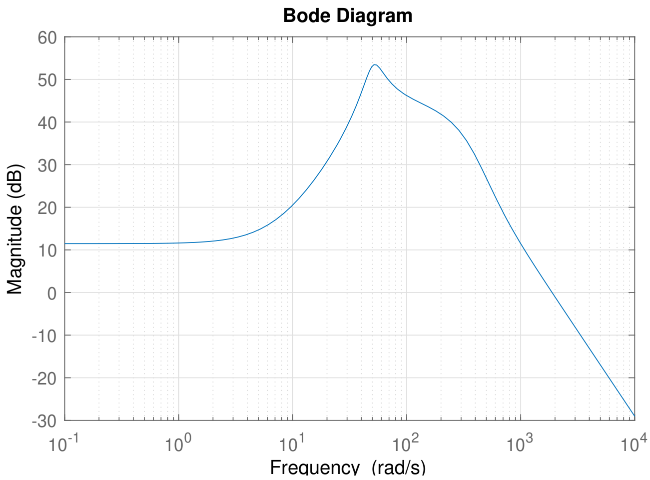

Figure 4.21: The bode plot of d to y_p

As can be seen in Figure 4.22, the closed loop system does not respond in high frequencies as it does in low frequencies, not to track the sensor noise, thus the noise is directly seen on the error.

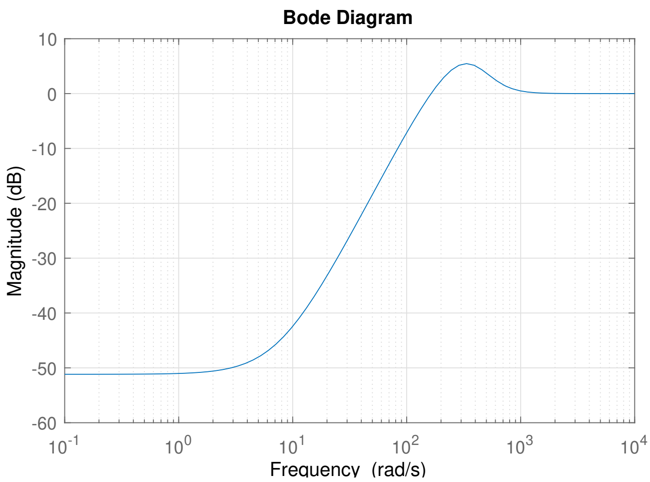

Figure 4.22: The bode plot of n to e

As given in the bode plot of n to u in Figure 4.23, the closed loop system does not respond in high frequencies not to track the sensor noise, thus the required controller input is small in higher frequencies. It is noted that the gain of the transfer function between n to u is lower than 0 dB for all low frequencies. This arises from the respective units of d $[A]$ and n $[N]$.

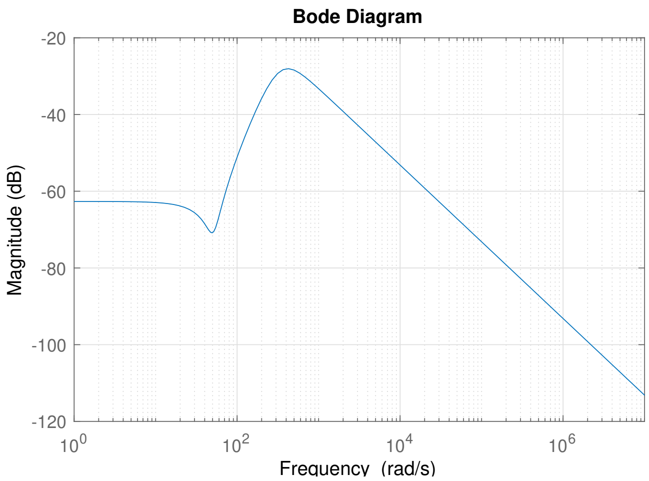

Figure 4.23: The bode plot of n to u

The bode plot of n to y_p is given in Figure 4.24. As can be seen in Figure 4.24, the closed loop system does not respond in high frequencies, thus the noise is not effective on the error in high frequencies.

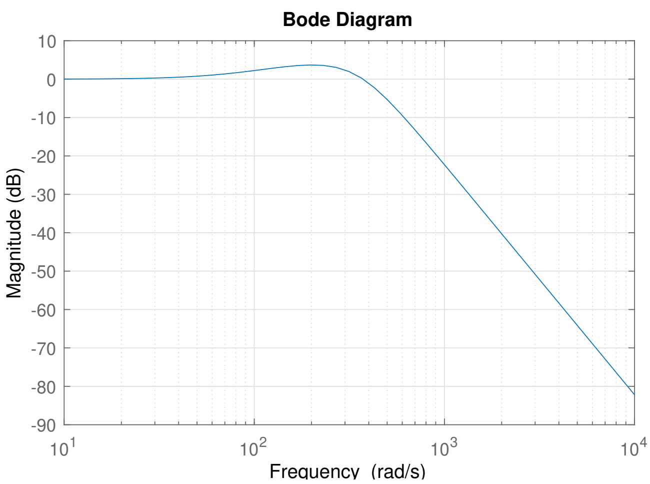

Figure 4.24: The bode plot of n to y_p

4.7 Robust Stability and Robust Performance

4.7.1 Robust Stability

The criterion for nominal stability using Nyquist theorem is that the loop gain of the system should not encircle the point -1 for the whole frequency range on the Nyquist plot as shown in Figure 4.25.

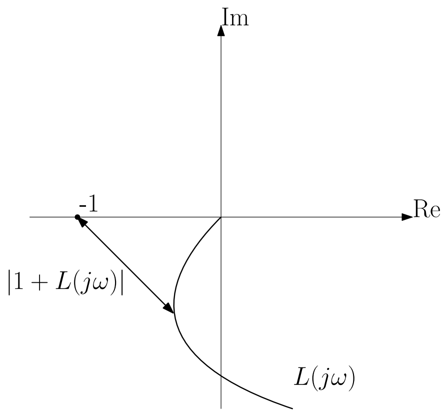

Figure 4.25: The nominal stability criterion on Nyquist plot

However for *Robust Stability*, loop gains of all perturbed systems $(L_p(j\omega))$ should not encircle -1 on the real axis of Nyquist plot for the whole frequency range as in Figure 4.26.

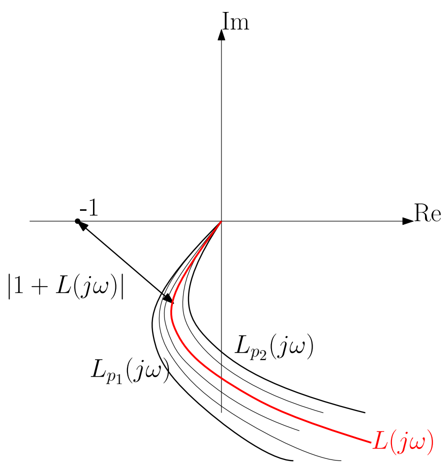

Figure 4.26: The robust stability criterion on Nyquist plot

Here, one can remember the nominal generalized plant as in Figure 4.5. In order to represent the perturbed plant, a block Δ, which is called as uncertainty, is added to the system. Then, general problem in H_∞ controller, together with controller and uncertainty can be shown as in Figure 4.27.

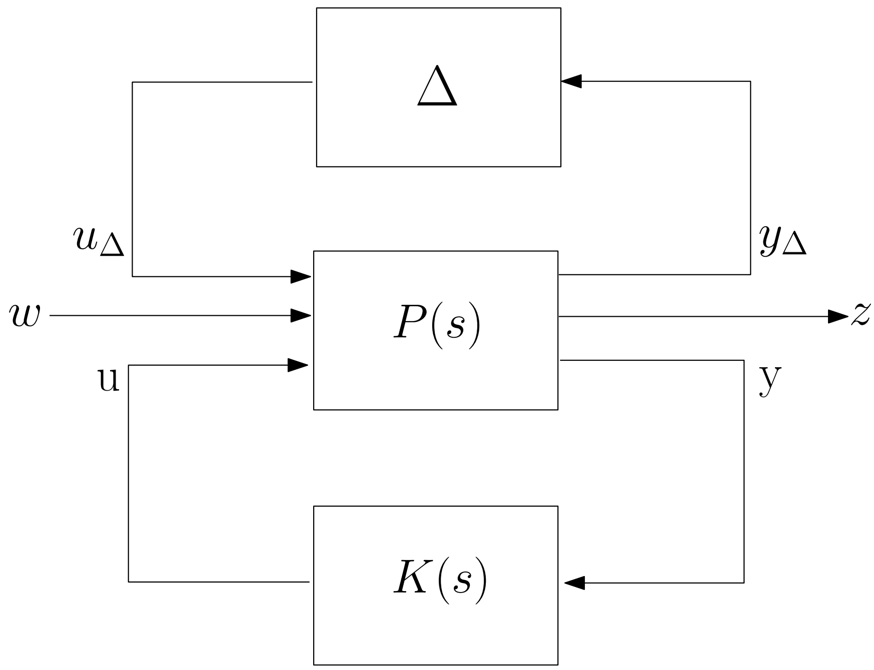

Figure 4.27: Generalized plant with controller and uncertainty

By using the expressions between eqn. 2.31 and eqn. 2.32, the Lower LFT of $P(s)$ with $K(s)$, named as N, is found as

$$N = F_l(P, K) \tag{4.31}$$

Then, we are left with the generalized plant with the uncertainty as in Figure 4.28.

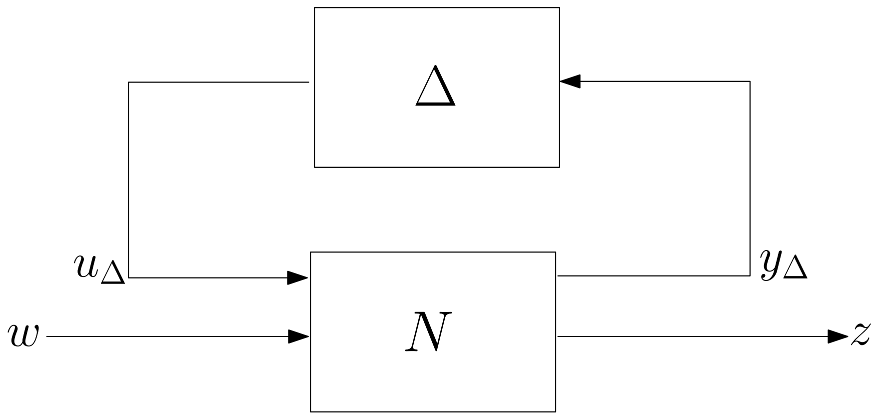

Figure 4.28: Generalized plant with uncertainty

If the upper LFT of the structure in Figure 4.28 is considered, the result is

$$F_u(N,\Delta) = \left[N_{22} + N_{21}\Delta(I - N_{11}\Delta)^{-1}N_{12}\right] \tag{4.32}$$

Here, if the Δ block and the nominal system N is assumed to be stable, and also remembering eqn. 2.33 the only instability can be caused by $(I - N_{11}\Delta)^{-1}$ which lies on the feedback line [41]. Here, in eqn. 4.32, the transfer function from all outputs (w) to the inputs (z) of uncertainty block Δ can be denoted by $M = N_{11}$ as in Figure 4.29.

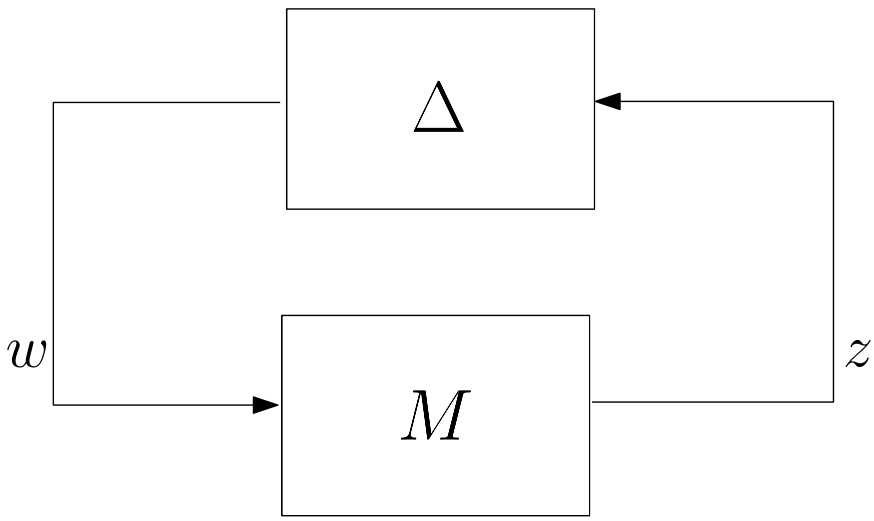

Figure 4.29: Generalized plant with uncertainty

For unstructured Δ blocks, meaning that Δ could be in any form ensuring that $\|\Delta\|_\infty < 1$, and using small gain theorem, the robust stability condition for unstructured Δ becomes:

$$RS \Rightarrow \bar{\sigma}(M(j\omega))\bar{\sigma}(\Delta(j\omega)) < 1 \tag{4.33}$$

The Δ block, stands for the uncertainties. Since it represents the component level uncertainties (that is uncoupled) in the scope of this thesis, this block has a diagonal structure as in eqn. 4.34.

$$\Delta = \begin{bmatrix} \Delta_1 & 0 & \cdots & 0 \\ 0 & \Delta_2 & \cdots & 0 \\ \vdots & \vdots & \ddots & \vdots \\ 0 & 0 & \cdots & \Delta_n \end{bmatrix} \tag{4.34}$$

When the Δ block is structured as in eqn. 4.34, the RS condition becomes:

$$RS \quad if \quad \bar{\sigma}(M(j\omega)) < 1 \tag{4.35}$$

Also for the $M\Delta$ structure given in Figure 4.29, the stability is guaranteed if:

$$det(I - M\Delta(j\omega)) \neq 0 \tag{4.36}$$

In order to check the amount of *"robustness"* of the system, the $Structured\ Singular\ Value\ \mu$ is defined as the inverse of the minimum of the largest singular value of Δ ($\bar{\sigma}(\Delta)$), which makes $(I - M\Delta)$ singular for structured Δ.

$$\mu(M) = \frac{1}{min\left\{\bar{\sigma}(\Delta) : det(I - M\Delta) = 0\right\}} \tag{4.37}$$

The $Structured\ Singular\ Value\ \mu$ can also be defined by normalizing the Δ by a factor of k_m and looking for the smallest k_m value which makes $(I - k_m M\Delta)$

singular, such that:

$$\mu(M) = \frac{1}{min\left\{k_m : det(I - k_m M\Delta) = 0\right\}} \tag{4.38}$$

The robustness of the system can be graded depending on how small the μ value is. Lower μ value means the system is more robust, while $\mu = 1$ means that there is a singularity with $\bar{\sigma}(\Delta) = 1$ and this singularity yields to instability.

4.7.2 Robust Performance

The criterion for robust performance using Nyquist theorem is that loop gains of all perturbed systems should not enter the disc around -1,for the whole frequency range, which is defined by the performance weight (W_p) on the real axis of Nyquist plot as illustrated in Figure 4.30.

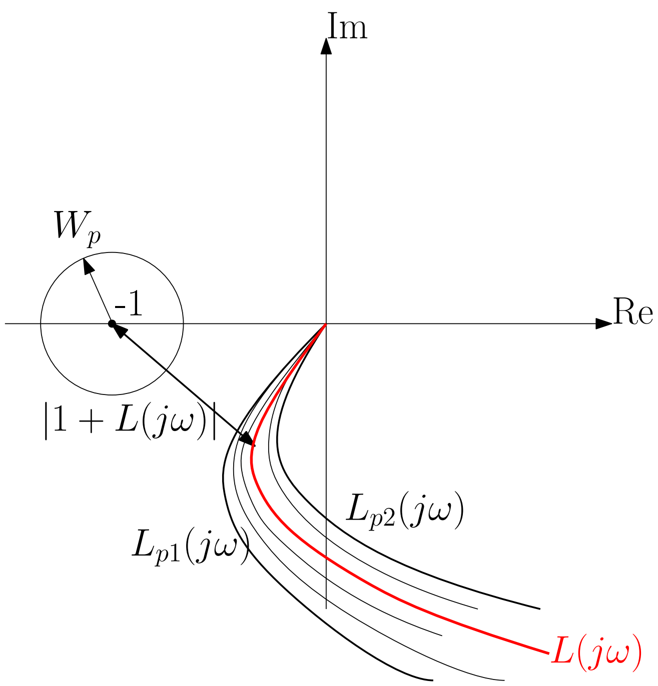

Figure 4.30: The robust performance criterion on Nyquist plot

Here, one can remember the general control problem visualized in Figure 4.27. Again, the lower LFT of the $P(s)$ with $K(s)$ gives us the $N\Delta$ structure given in Figure 4.28.

A fictitious block on the performance channel is added in order to close the loop as in Figure 4.31. This block stands for the performance specifications of the system.

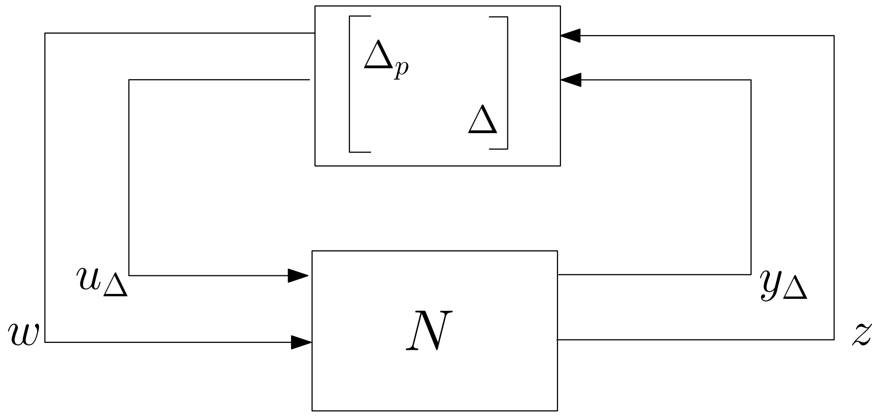

Figure 4.31: Uncertainty block with fictitious Δ_p

In this case, $\hat{\Delta}$ is in the diagonal form as shown in eqn. 4.39, where Δ_p is a full matrix.

$$\hat{\Delta} = \begin{bmatrix} \Delta_p & 0 & \cdots & 0 \\ 0 & \Delta_1 & \cdots & 0 \\ \vdots & \vdots & \ddots & \vdots \\ 0 & 0 & \cdots & \Delta_n \end{bmatrix} \tag{4.39}$$

When we have this structure given in Figure 4.31, the *Robust Stability* criterion of this $N\hat{\Delta}$ structure actually gives the *Robust Performance* characteristic of the system. This means that, the *Robust Performance* of the system can be tested by looking at the $Structured\ Singular\ Value$ of this new structure, that is:

$$RP \quad if \quad \mu_{\hat{\Delta}}(N(j\omega)) < 1 \tag{4.40}$$

To sum up all stability and performance characteristics, with the help of Figure 4.31, following expression can be derived, by partitioning N:

$$\begin{bmatrix} z \\ y_\Delta \end{bmatrix} = \begin{bmatrix} N_{11} & N_{12} \\ N_{21} & N_{22} \end{bmatrix} \begin{bmatrix} w \\ u_\Delta \end{bmatrix} \tag{4.41}$$

From this expression, all performance and stability conditions can be written such that:

$$\begin{aligned} Nominal\ Stability &\Leftrightarrow N\ is\ internally\ stable \\ Nominal\ Performance &\Leftrightarrow \mu_{\Delta_p} = \bar{\sigma}(N_{22}) < 1\ and\ Nominal\ Stability \\ Robust\ Stability &\Leftrightarrow \mu_{\Delta}(N_{11}) < 1\ and\ Nominal\ Stability \\ Robust\ Performance &\Leftrightarrow \mu_{\hat{\Delta}}(N) < 1\ and\ Nominal\ Stability \end{aligned} \tag{4.42}$$

4.7.3 Robust Stability and Performance Analysis

For the force excitation system, the parameters which could have uncertain values are:

- The torque constant of the Electric Motor K_t can attain different values depending on conditions such as temperature and current density. From the datasheet and also by tests, the uncertainty for K_t is 5 %.
- The viscous damping coefficient B can have different values depending on the temperature and speed. The uncertainty for B is 15 % from different system identification results.
- The spring coefficient k can have different values due to its nonlinear behavior in some regions. The uncertainty is calculated for k from tests is 5 %.

By using this uncertainty values the perturbed system is constructed via using MATLAB's *"sysic"* command. Then, by using *"robuststab"* command on MATLAB, the Robust Stability of the system checked by μ analysis. The result is found as follows:

- System is robustly stable for the modeled uncertainty.
- The system can tolerate up to 951% of the modeled uncertainty.
- The perturbation which will destabilize the system is 964% of the modeled uncertainty.

- The instability caused by this perturbation occurs at the frequency 49.4 rad/seconds.

With the synthesized controller and the identified plant, the SSV of the system for *"RS"* over the whole frequency spectrum can be plotted as in Figure 4.32.

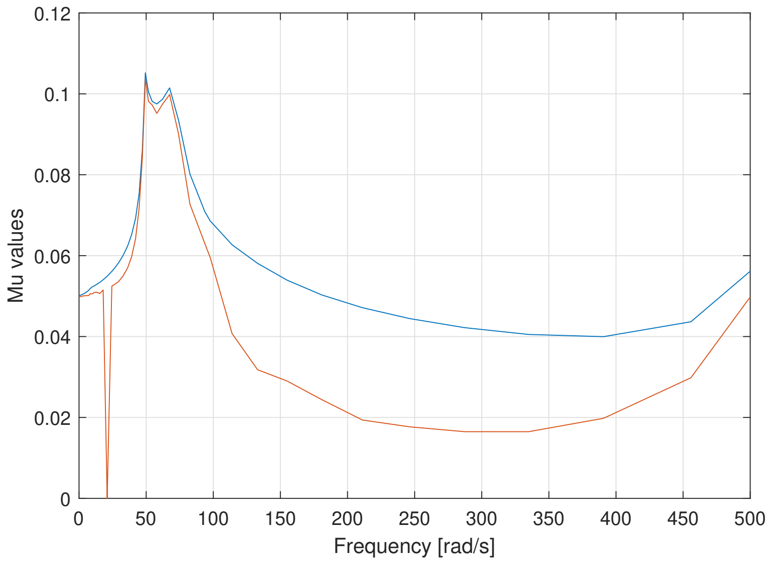

Figure 4.32: Structured singular values for RS

Figure 4.32 shows that, the SSV (μ) values are below 1 all over the frequency range, having a peak at 49.4 rad/seconds. This means that stability is guaranteed for all frequencies with a relatively large margin.

Also by using the uncertainty values and the defined weightings, the perturbed system is again constructed via using MATLAB's *"sysic"* command. Then, by using *"robustperf"* command on MATLAB, the result for RP is turned out to be:

- Uncertain system achieves performance robustness to modeled uncertainty.
- The tradeoff of model uncertainty and system gain is balanced at a level of 100 % of the modeled uncertainty.
- A model uncertainty of 100% can lead to input/output gain of 0.998 at 54.5 rad/seconds.

Also to visualize, the *Structured Singular Values* for RP can be seen as in Figure 4.33.

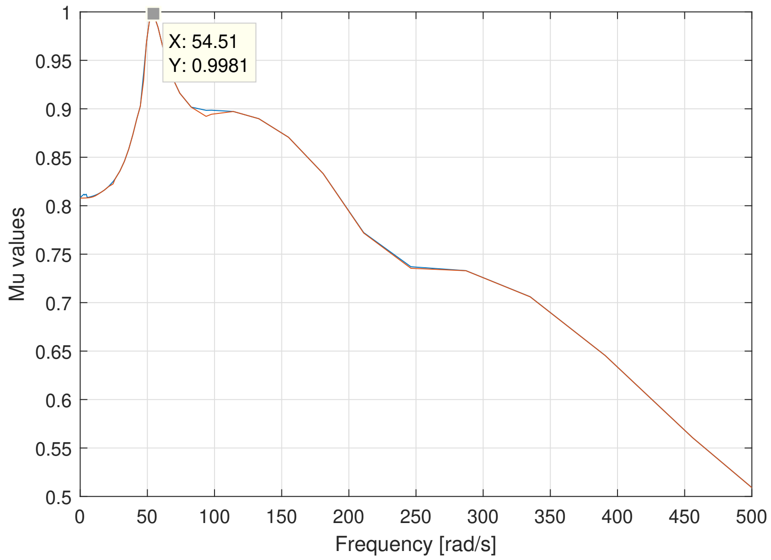

Figure 4.33: Structured singular values for RP

Figure 4.33 indicates that, the SSV (μ) values are below 1 all over the frequency range, having a peak at 54.5 rad/second. This means that the performance of the system is guaranteed for all frequencies, however, with a relatively less margin at 54.5 rad/second. Also, this value is quite close to the bandwidth of the system. Therefore, a higher uncertainty level than defined may lead to loss of performance and additional care must be given while working around this frequency band. However, the stability is still guaranteed for a greater margin as discussed before.

4.8 Feedforward Compensation

With the controller structure given in Figure 4.2, it is assumed that only the model of force control system is known, and no other information is available. However, the variables of the opposing system are also known, such as the position, speed, and current. By making use of this information, the performance of the system can be improved.

The most critical objective on force control is disturbance rejection. Without feedforward compensation, the disturbance is noticed only when the position disturbance is affecting the load and, consequently, the error. However, since the position control systems reference, output position, output speed, and the current is available, these can be used for feedforward compensation.

Because of the speed difference of two systems, an undesired force, which could be named as *"surplus force"* occurs. If the speeds of both systems are synchronized, or the speed information is fed forward to the force control system, this surplus force could be minimized. One way to do this is feeding the reference speed directly to the force control system. However, the drawback is, speed tracking is not good enough, and this may lead to another undesired force on the output. Feeding the measured speed is a better option, yet, since it is not directly measured and derived from position, some delay and noise is inevitable. Another option is to use the current command of the position control system for feedforward structure [8]. Since the two systems are similar and they use the same electric motor at each end, this could be done by filtering (or scaling) the current of the position control system and feeding it to the FES directly. We also know that the current is proportional with the torque and consequently acceleration, thus, the upcoming acceleration information will be fed forward to the FES and the speed synchronization will be improved. Also this structure can be presented as in Figure 4.34.

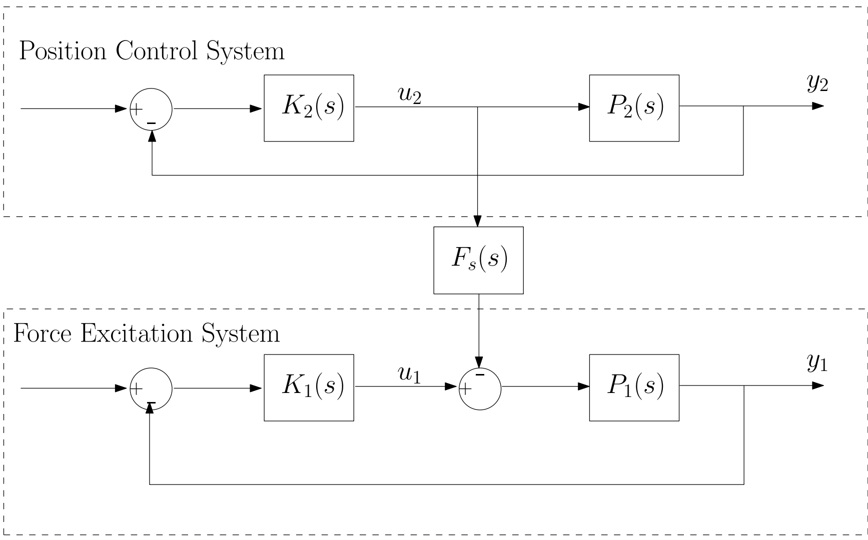

Figure 4.34: Feedforward structure

The transfer function of position control part is available and its identification is out of the scope of this thesis. The transfer function of position control system from current to position is given as:

$$P_2(s) = \frac{\theta(s)}{I(s)} = \frac{375}{s(0.76s+1)} \tag{4.43}$$

Also the transfer function of force excitation part is found as in eqn. 3.24. In order to find the scaling filter $F_s(s)$, these transfer functions are proportioned as

$$F_s(s) = \frac{P_2}{P_1} = \frac{\frac{375}{s(0.76s+1)}}{\frac{750}{s(0.054s+1)}} = \frac{20.25s^2 + 375s}{570s^2 + 750s)} \tag{4.44}$$

The bode graph of the filter is as given in Figure 4.35:

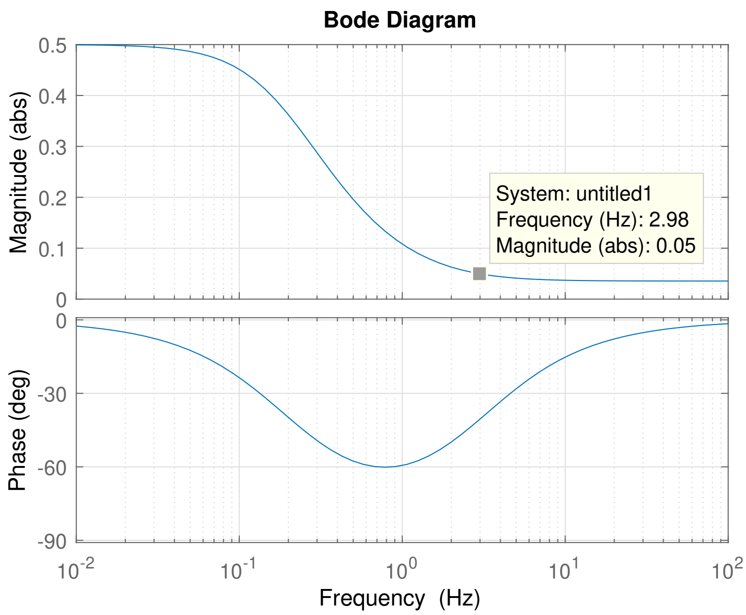

Figure 4.35: Bode graph of feedforward filter

Since this feedforward action will be mainly used on high frequency range assuming that the low frequency disturbances are compensated by FES itself, and also for simplicity, rather than using the transfer function, an average value of the magnitude ratio is used as:

$$F_s(s) = 0.05 \tag{4.45}$$

The effect of feedforward compensation will be discussed in the simulations and experimental results in detail in Section 5.

CHAPTER 5

SIMULATION RESULTS AND EXPERIMENTAL EVALUATION

In this section, in order to see the results with the designed controller, a set of simulations are carried out and also the experimental results are evaluated. Both systems are performing simultaneously for both simulation and experimental environment.

5.1 Simulation Results

In order to see the nominal performance of the system, a set of simulations are performed in MATLAB-Simulink environment. The illustration of the block diagram for simulation can be seen on Figure 5.1. Here, on FES, the synthesized H_∞ controller is used while on position control system a Model Predictive Controller, whose design is not included in this thesis, is used.

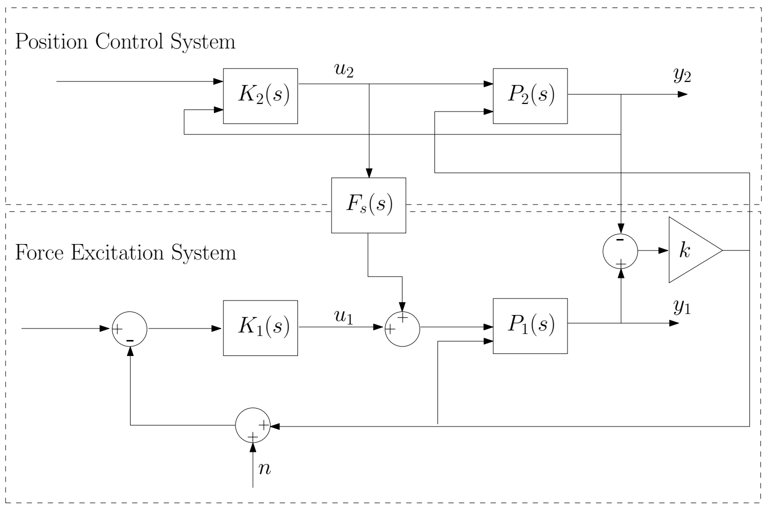

Figure 5.1: Block diagram for simulation

The references for FES and position control system can be seen on Figure 5.2. In the simulations and also on experimental results, the points t=1s (for step response of FES), and t=2s (for disturbance rejection of FES) are examined.

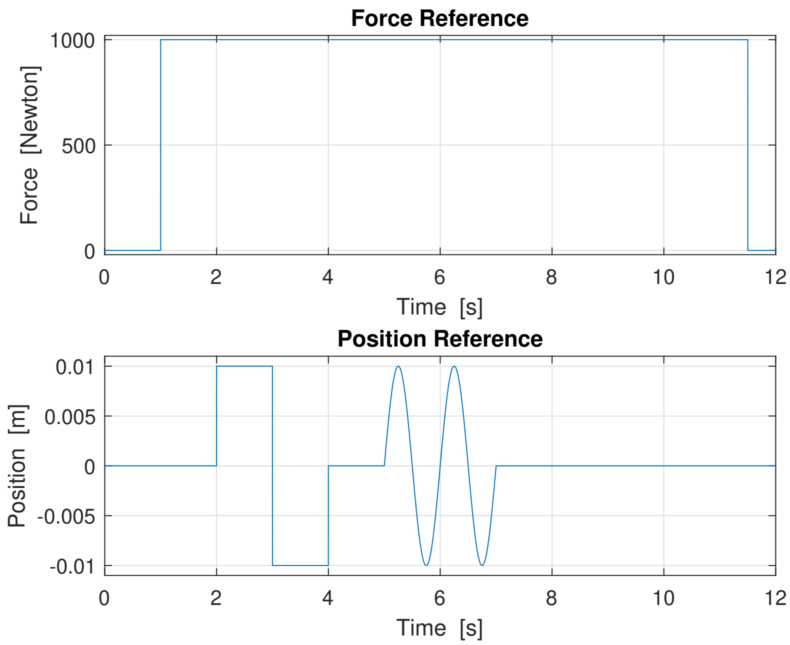

Figure 5.2: The references for both systems

The step command In Figure 5.2 is smoothened with at most $20000 \mathrm{N/s}$ force rate limit to avoid instantaneously infinite increase of derivative of the step command. It is also noted that the command for position control system is constrained with the value which corresponds to 1000 rpm speed limit from this point on. The sampling time used on simulations and also on experimental system is 1000 Hz, which is high enough as compared to the bandwidth of the closed look system.

For the system with no feedforward compensation, the step response for a reference command of 1000 N is given in Figure 5.3. In this simulation, the position control system is holding the shaft of the tested ballscrew stationary for the first 2 seconds.

As in Figure 5.3, the overshoot is less than 10 percentage of the final value and the settling time is less than 15 milliseconds (according to 2% settling time criterion) for the specified step command.

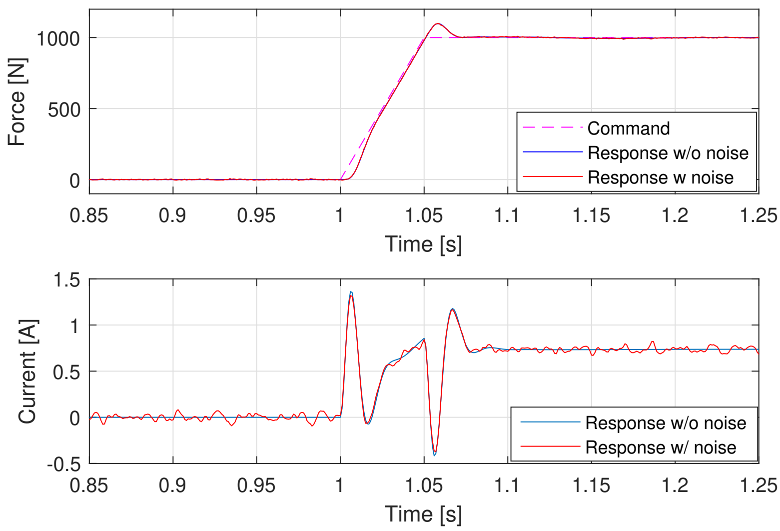

Figure 5.3: Step response of the system

Another important metric is the disturbance rejection for this system. In Figure 5.4, the response of the system for a disturbance input of 5 mm which is the linear movement of the position control system, at t $= 2$s can be seen, while the system already has 1000 N force on itself.

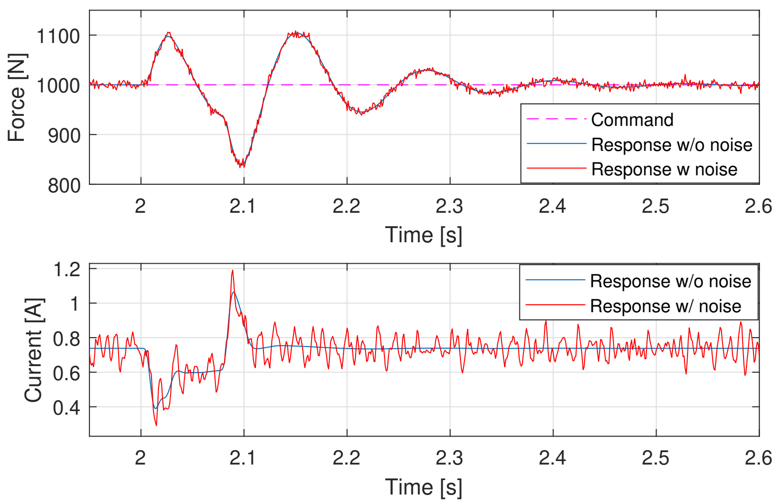

Figure 5.4: Disturbance rejection of the system for 5 mm linear movement

As can be seen in Figure 5.4, the maximum deviation from the force reference for this disturbance is around 100 N and dies out in 0.35 s.

The force measurement device in this system is load cell with analog output. Like all other analog devices, load cells stream out noisy data. A sample measurement result from the load cell with no load on it can be seen in Figure 5.5. As we can see, the noise is in a 25 N band. A Gaussian distributed random noise, with zero mean and variance of 10 is injected in order to simulate the noise of the utilized sensor to the measured output in the simulation. The same simulations are carried out, and the results are also given in Figure 5.3 and Figure 5.4.

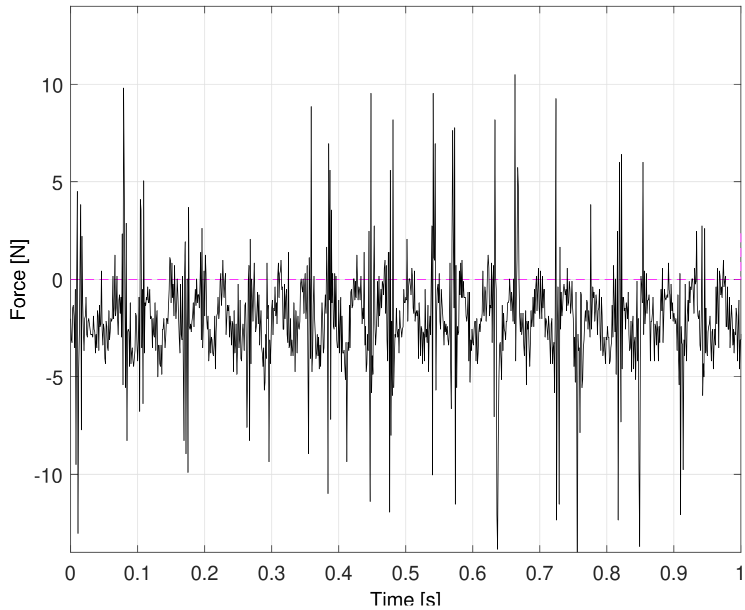

Figure 5.5: Noise characteristics of the load cell

As can be seen from the Figure 5.3and Figure 5.4, the response to the noise can be regarded as very low relative to the final value of the step command and the noise does not cause any vibration and instability on the system.

For a better disturbance rejection, feedforward compensation is integrated to the closed loop system as in Figure 4.34 and the effect of the feedforward compensation is seen in the simulation environment. In Figure 5.6 the response of the system with the feedforward compensation to the 5 mm position disturbance is given, while the reference command is 1000 N.

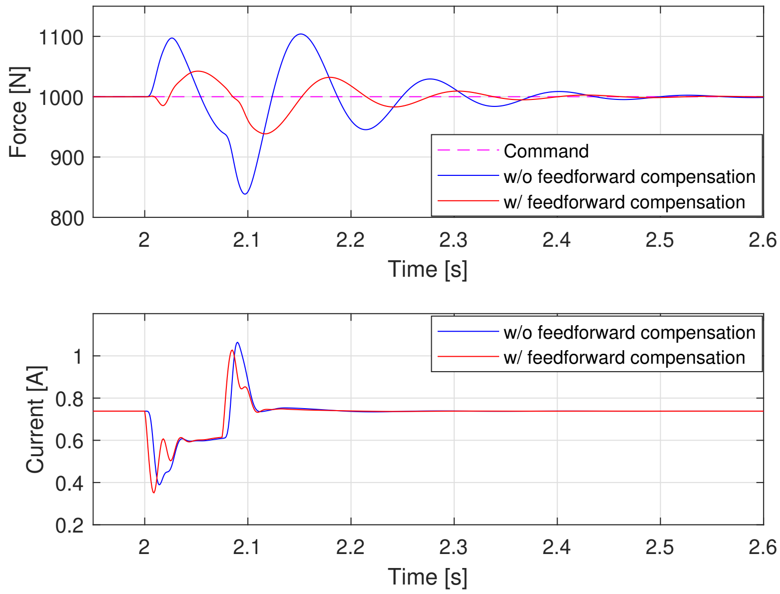

Figure 5.6: Disturbance rejection of the system with feedforward compensation, 5 mm disturbance

In Figure 5.7 the response of the system with the compensation to the 10 mm position disturbance is given, while the reference command is 1000 N.

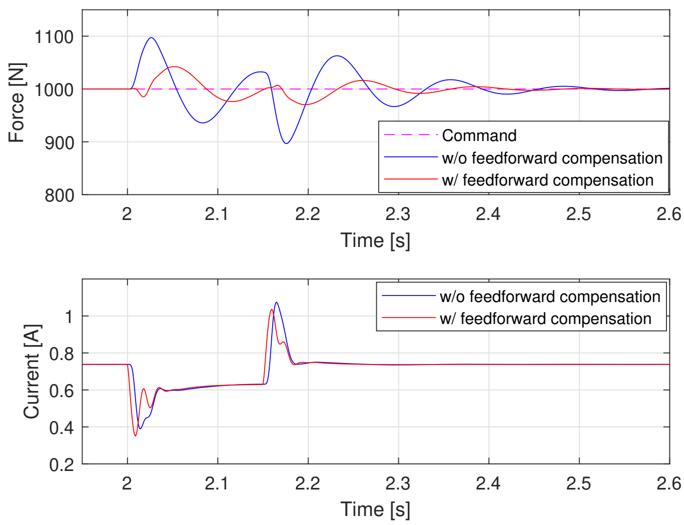

Figure 5.7: Disturbance rejection of the system with feedforward compensation, 10 mm disturbance

As can be seen from the Figures 5.6 and 5.7, the maximum deviation from the reference decrease regarding to the closed loop system without feedforward compensation so that the force tracking is much better.

In addition to the given simulation results above, the simulations regarding parameter uncertainties are performed. With the defined uncertainties for parameters, which are, 5% change in the spring constant value k, 15% change in the viscous damping B and 5% change in the torque constant K_t, a number of simulations are performed by randomly changing the uncertain parameters in their uncertainty range. The uncertain system response for the 5 mm position disturbance can be seen in Figure 5.8.

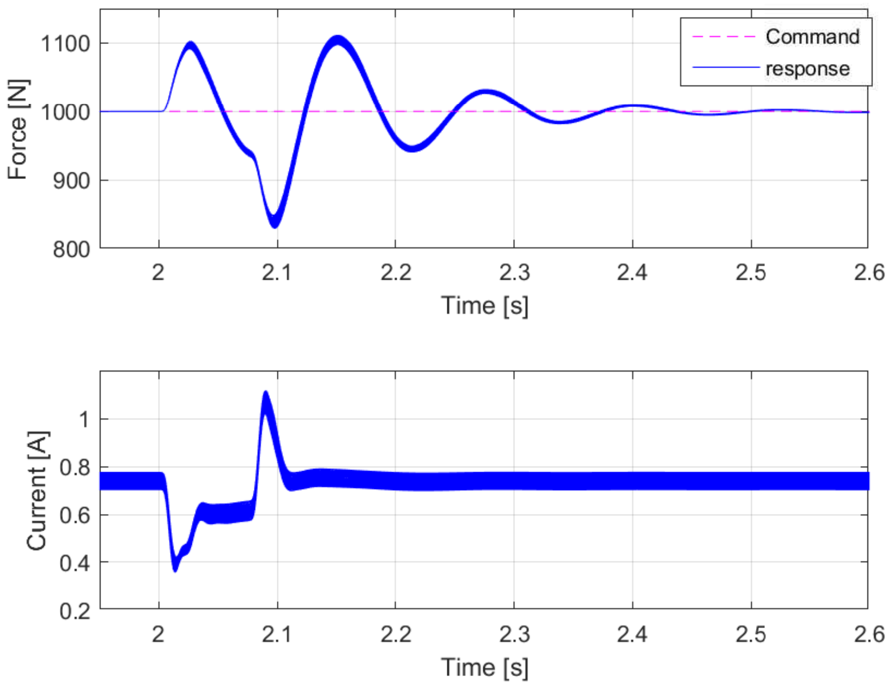

Figure 5.8: Disturbance rejection of the system with sets of parameter uncertainties, 5 mm disturbance

The same set of simulations are also carried out with the addition of the noise in order to approximate the real case. The uncertain system response for the 5 mm position disturbance and noise input can be seen in Figure 5.9.

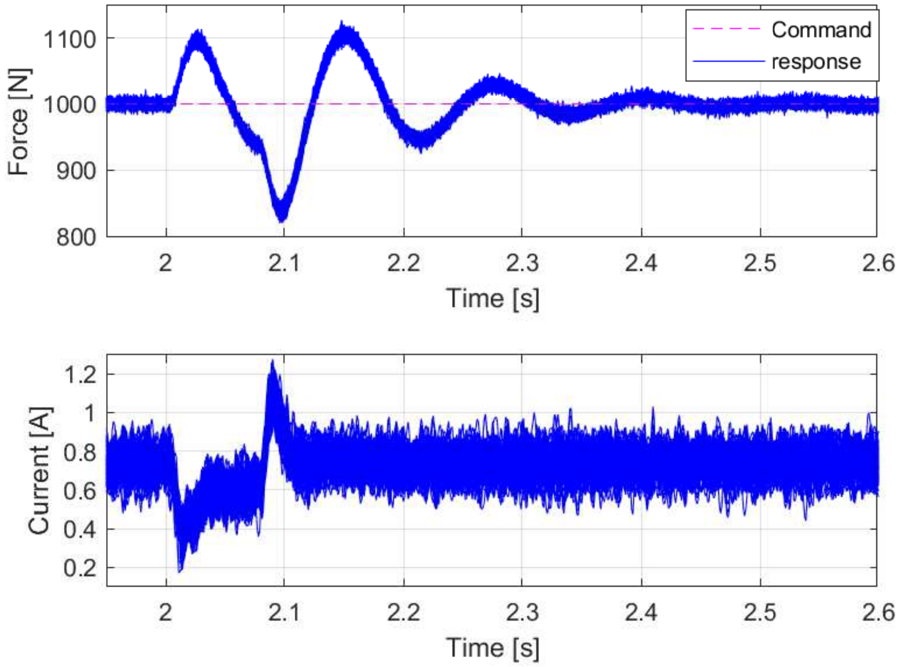

Figure 5.9: Disturbance rejection of the system with sets of parameter uncertainties and noise addition, 5 mm disturbance

As can be seen from the Figures 5.8 and 5.9, the responses are similar for the corresponding responses with nominal parameters and the given uncertainty does not cause instability on the system. The effect on the input is greater, yet, still in the admissible range.

5.2 Experimental Test Setup and the Results

5.2.1 Experimental Test Setup

The experimental setup consists of the components below

- Host Computer
- Target Computer
- Test Rig.

The schematics of the experimental setup is given in Figure 5.10.

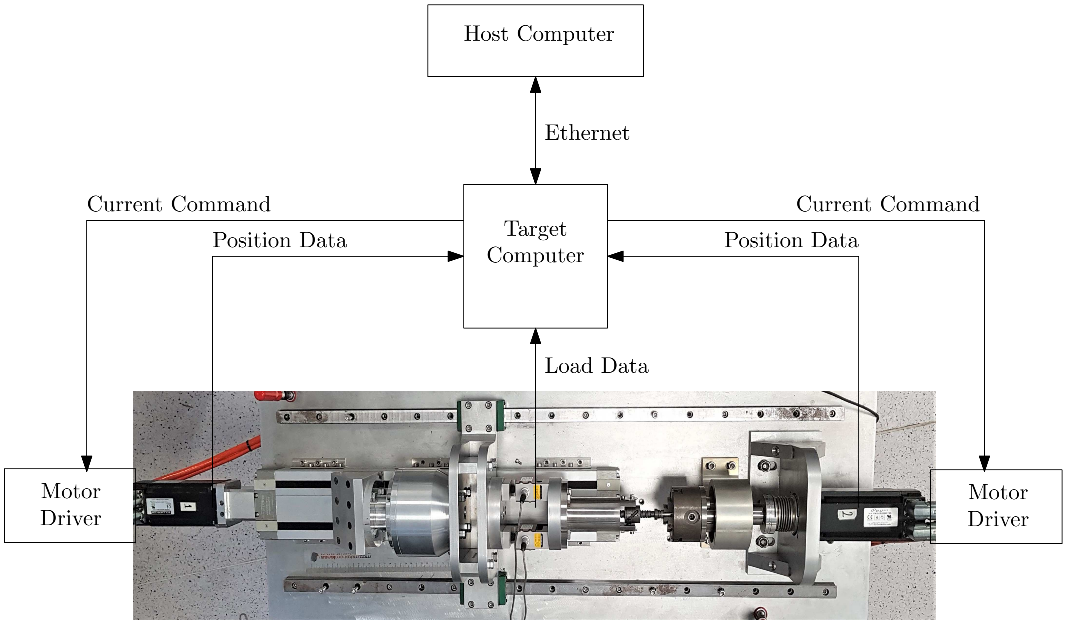

Figure 5.10: The experimental setup

The host computer manage the whole system via MATLAB and its toolbox. On the host computer, the position and force commands as well as the project file is created. Then these commands are sent to the target computer via ethernet card and cable for real-time operation. The target computer has data acquisition cards installed on itself. After the MATLAB Simulink files are uploaded to the target computer, the real-time operation starts. One position control loop for position control system and one force control loop for FES are run on the target computer.

As a closed loop iteration process for the force control part in one sampling interval, the controller computes the required current for the closed-loop control and sends it to the servo driver through an analog channel. The driver commutes the electric motor and causes movement. The resulting force is retrieved by the load cell and sent back to the target computer via an analog channel. Depending on the measured output, a new current command is computed by the controller for the next loop.

Similarly, for the position control part, the controller computes the required current for closed-loop control and sends it to the servo driver through an analog channel. The driver commutes the electric motor and causes movement. The resulting position of the ball screw shaft is retrieved by the encoder and sent back to the target computer via a digital channel. Then, a new current command is computed by the controller for the next loop.

5.2.2 Experimental Results

In order to evaluate the performance of the designed system in real time, a number of experiments are carried out on the setup. Same references given as in Figure 5.2 to the system and the results are discussed in this section.

For the system with no feed-forward compensation, the step response for a force command of 1000 N is given in Figure 5.11.

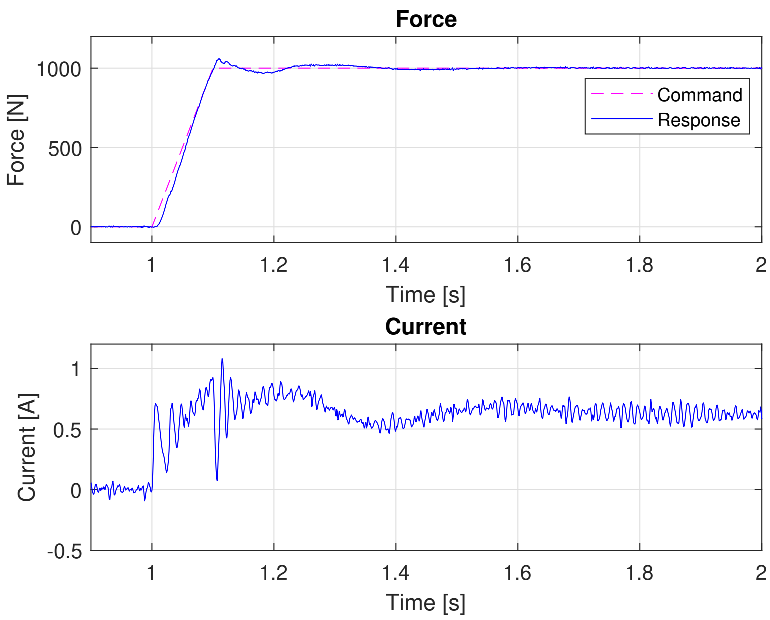

Figure 5.11: Step response of the system

In Figure 5.12, the response of the system with no feed-forward compensation for a disturbance input of 5 mm linear movement of the position control system at t $= 2$s can be seen, while the system already has 1000 N force on itself.

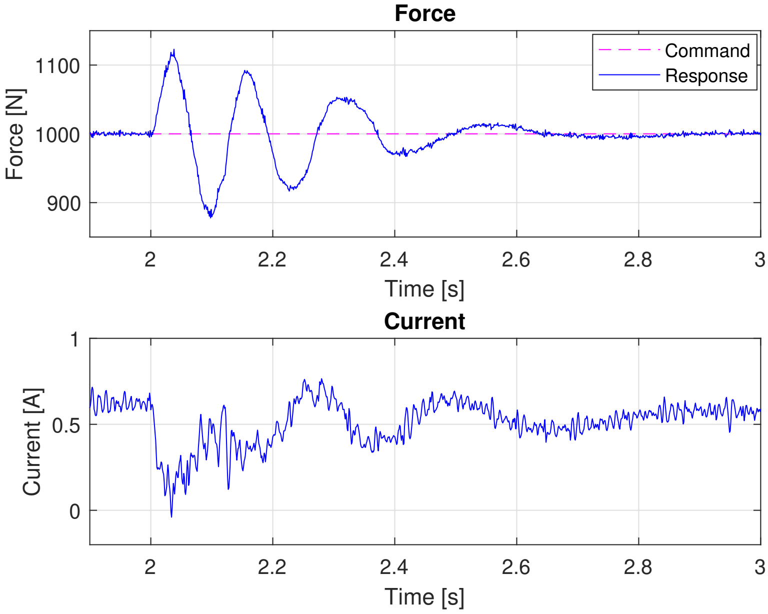

Figure 5.12: Disturbance rejection of the system for 5 mm disturbance

In Figure 5.13, the response of the system with no feed-forward compensation for a disturbance input of 10 mm linear movement of the position control system at t $= 2$s can be seen, while the system already has 1000 N force on itself.

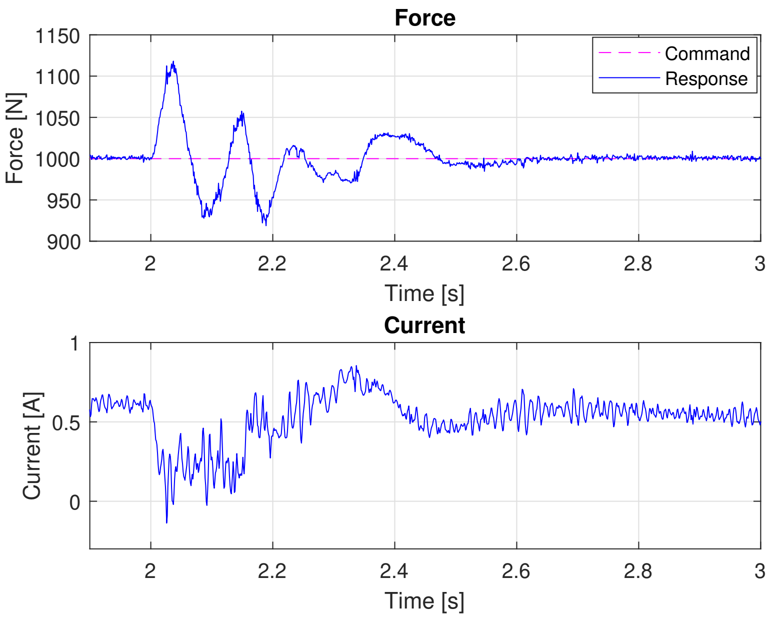

Figure 5.13: Disturbance rejection of the system for 10 mm position disturbance

As can be seen in Figures 5.12 and 5.13, the maximum deviation from the reference for this disturbance is around 100 N and dies out in 0.45 s which is determined around 0.35 s in simulations in Section 5.1. The small difference arises from linearly estimated nonlinear dynamics of the system in Section 3.3.

In Figure 5.14 the response of the system with the feedforward compensation to the 5 mm position disturbance is given, while the reference command is 1000 N.

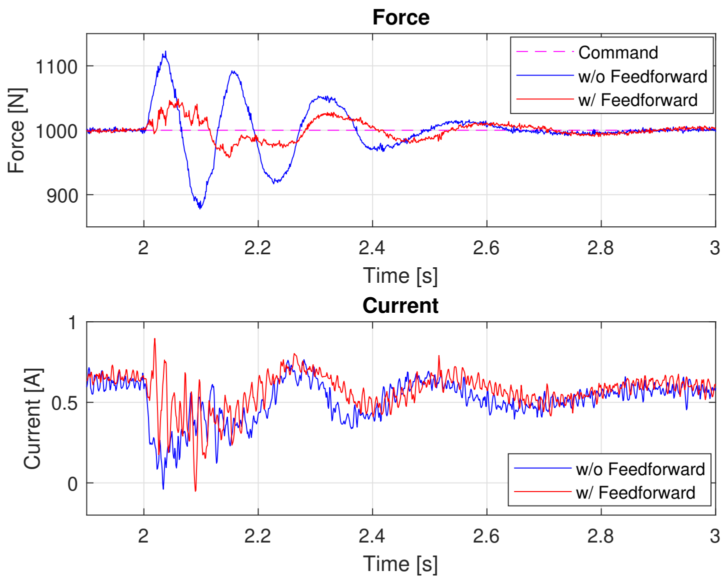

Figure 5.14: Disturbance rejection of the system for 5 mm position disturbance with feed forward compensation

In Figure 5.15 the response of the system with the feed-forward compensation to the 10 mm position disturbance is given, while the reference command is 1000 N.

As can be seen from the Figures 5.14 and 5.15, the maximum deviation from the reference and the settling time of the transition region decrease regarding to the closed loop system without feed-forward compensation.

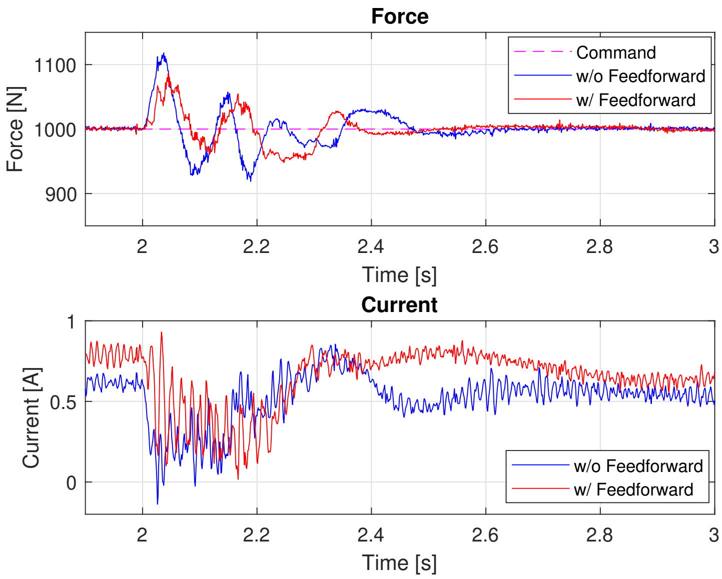

Figure 5.15: Disturbance rejection of the system with feedforward compensation, 10 mm disturbance

As a last step, the bandwidth of the system is experimentally evaluated and the response for 12 Hz sine signal can be seen as in Figure 5.16. The amplitude ratio is just above 0.707 which corresponds to -3 dB decrease.

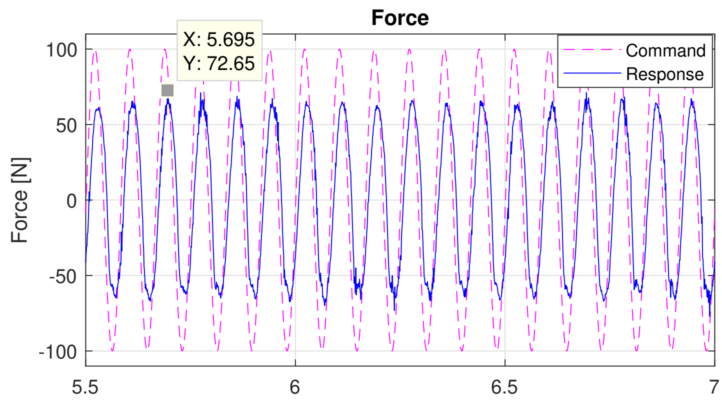

Figure 5.16: Experimental bandwidth of the system

CHAPTER 6

CONCLUSIONS AND FUTURE WORK

6.1 Conclusions

Ball screws are components used to convert the rotary motion into linear motion with relatively high mechanical efficiency. In the scope of the thesis, a test rig is designed to test and verify the dynamic load capacity of ballscrews with variable rotational speeds and load factors. Furthermore, mathematical modeling of the test rig is derived, and the coefficients of the derived model are estimated through system identification principles by utilizing experimental data. Moreover, a robust force controller is synthesized for the force excitation system which exerts load on the ballscrews, and the mathematical model of the closed loop system under the effect of uncertainties is analyzed in the simulation environment. Lastly, the surplus force caused by the axial movement of the ballscrews during simultaneous motion and loading is highly eliminated through proposed feedforward controller. The simulation and experimental results show the efficacy of the designed robust force feedback and the proposed feedforward compensation together on the system with model uncertainties and on the identified system.

With this proposed test setup, custom ball screws can be tested with real scenarios at the subcomponent level. In the scope of this study, force excitation part of this test setup is discussed. The design of the test rig is reviewed, and the system identification of the force excitation part has been made. A robust H_∞ controller is designed theoretically with the identified model, and the robustness with respect to uncertain parameters is analyzed by using μ analysis method. In this analysis, the system is turned out to be robustly stable and can tolerate the defined uncertainty levels in its operating frequency band.

The designed H_∞ controller rejects the disturbance arising from the relative movement of FES and position control system with the desired performance. Besides, the proposed feedforward compensator, which uses the current command of the position control system, contributes to the disturbance rejection and increases the performance of the system for both simulations and the real-time operations.

6.2 Future Works

The following items are recommended as future work:

- Increasing the performance of the position control part by redesigning the system and reducing the relatively high inertia caused by coupling parts.
- Estimating the force by using an observer and minimizing the noise problem due to force measurement. By doing that, a higher gain controller can be designed for enhanced performance.

REFERENCES

[1] G. A. Pratt, M. M. Williamson, P. Dillworth, J. Pratt, and A. Wright, “Stiffness isn't everything,” in *experimental robotics IV*, pp. 253–262, Springer, 1997.

[2] G. A. Pratt and M. M. Williamson, “Series elastic actuators,” in *Proceedings 1995 IEEE/RSJ International Conference on Intelligent Robots and Systems. Human Robot Interaction and Cooperative Robots*, vol. 1, pp. 399–406, IEEE, 1995.

[3] G.-q. Li, J. Cao, B. Zhang, and K.-D. Zhao, “Design of robust controller in electrohydraulic load simulator,” in *2006 international conference on machine learning and cybernetics*, pp. 779–784, IEEE, 2006.

[4] X. Wang and D. Feng, “A study on dynamics of electric load simulator using spring beam and feedforward control technique,” in *2009 Chinese Control and Decision Conference*, pp. 301–306, IEEE, 2009.

[5] T. Feng and C.-q. ZHAO, “Design and research of electric control load system of flight simulator,” *DEStech Transactions on Engineering and Technology Research*, no. iceea, 2016.

[6] N. Ullah, “Loads simulator system for testing and qualification of flight actuators,” *Recent Progress in Some Aircraft Technologies*, p. 77, 2016.

[7] Y. Jianyong, J. Zongxia, Y. Bin, Y. Shang, and D. Wenbin, “Nonlinear adaptive robust force control of hydraulic load simulator,” *Chinese Journal of Aeronautics*, vol. 25, no. 5, pp. 766–775, 2012.

[8] Z.-X. Jiao, J.-X. Gao, H. Qing, and S.-P. Wang, “The velocity synchronizing control on the electro-hydraulic load simulator,” *Chinese journal of aeronautics*, vol. 17, no. 1, pp. 39–46, 2004.

[9] A. Plummer, “Robust electrohydraulic force control,” *Proceedings of the Insti-*

tution of Mechanical Engineers, Part I: Journal of Systems and Control Engineering, vol. 221, no. 4, pp. 717–731, 2007.

[10] Y. Nam and S. K. Hong, "Force control system design for aerodynamic load simulator," *Control Engineering Practice*, vol. 10, no. 5, pp. 549–558, 2002.

[11] J. Xu, Y. Li, X. Pan, and G. Wang, "Adaptive predicting control for electrical load simulator," in *2016 13th International Conference on Ubiquitous Robots and Ambient Intelligence (URAI)*, pp. 437–441, IEEE, 2016.

[12] Y. Jia and Y. Jie, "Research on electric load simulator based on dual loop control," in *2018 IEEE 4th Information Technology and Mechatronics Engineering Conference (ITOEC)*, pp. 1933–1936, IEEE, 2018.

[13] C. Yadong, S. Liang, S. Jiafeng, and Q. Zhidong, "Surplus torque research on electric motor loading simulator using active disturbance rejection controller," in *2017 29th Chinese Control And Decision Conference (CCDC)*, pp. 5124–5130, IEEE, 2017.

[14] N. Ullah and S. Wang, "Torque controller design for electrical load simulator with estimation and compensation of parametric uncertainty," in *Proceedings of 2012 9th International Bhurban Conference on Applied Sciences & Technology (IBCAST)*, pp. 15–21, IEEE, 2012.

[15] Y. Huang, K. Chen, and J. Wei, "Robust controller design and experiment for electric load simulator," in *2010 3rd International Conference on Advanced Computer Theory and Engineering (ICACTE)*, vol. 3, pp. V3–236, IEEE, 2010.

[16] L. Zhihui, Z. Jiao, Y. Shang, and S. Wu, "Eliminate the surplus torque of electro-hydraulic load simulator using the actuator command dynamic compensation control," in *2016 IEEE Chinese Guidance, Navigation and Control Conference (CGNCC)*, pp. 2070–2075, IEEE, 2016.

[17] G. Di Rito, E. Denti, and R. Galatolo, "Robust force control in a hydraulic work-bench for flight actuators," in *2006 IEEE Conference on Computer Aided Control System Design, 2006 IEEE International Conference on Control Applications, 2006 IEEE International Symposium on Intelligent Control*, pp. 807–813, IEEE, 2006.

[18] D. Q. Truong, K. K. Ahn, K. J. Soo, and Y. H. Soo, "Application of fuzzy-pid controller in hydraulic load simulator," in *2007 International Conference on Mechatronics and Automation*, pp. 3338–3343, IEEE, 2007.

[19] K. K. Ahn, D. Q. Truong, and Y. H. Soo, "Self tuning fuzzy pid control for hydraulic load simulator," in *2007 International Conference on Control, Automation and Systems*, pp. 345–349, IEEE, 2007.

[20] Q. Feng, G. Xiaoqiang, Y. Bo, and P. Zhongcai, "Theoretical analysis of surplus torque in electro-hydraulic load simulator," in *Proceedings of 2011 International Conference on Fluid Power and Mechatronics*, pp. 150–153, IEEE, 2011.

[21] S. Yang and W. Jianli, "The influence and compensation of gear backlash on electric load system," in *2017 2nd International Conference on Frontiers of Sensors Technologies (ICFST)*, pp. 479–483, IEEE, 2017.

[22] Z. Fan, X. Yu, L. Lu, P. Cheng, and R. Yang, "A self-adaptive synchronous servo compensation mechanism for redundant force suppression in aerodynamic loading system," in *2018 International Conference on Intelligent Autonomous Systems (ICoIAS)*, pp. 180–184, IEEE, 2018.

[23] C. Luo, J. Yao, and Q. Xu, "Extended state observer based nonlinear adaptive robust control of hydraulic load simulator," in *2016 35th Chinese Control Conference (CCC)*, pp. 4573–4578, IEEE, 2016.

[24] H. Anton and C. Rorres, *Elementary Linear Algebra, Binder Ready Version: Applications Version*. John Wiley & Sons, 2013.

[25] R. Henstock, "Linear analysis," *BOOK REVIEWS*, vol. 11, p. 1, 1967.

[26] B. Noble, J. W. Daniel, *et al.*, *Applied linear algebra*, vol. 3. Prentice-Hall New Jersey, 1988.

[27] G. H. Golub and C. Reinsch, "Singular value decomposition and least squares solutions," in *Linear Algebra*, pp. 134–151, Springer, 1971.

[28] K. Zhou, J. C. Doyle, K. Glover, *et al.*, *Robust and optimal control*, vol. 40. Prentice hall New Jersey, 1996.

[29] Z.-P. Jiang, A. R. Teel, and L. Praly, "Small-gain theorem for iss systems and applications," *Mathematics of Control, Signals and Systems*, vol. 7, no. 2, pp. 95–120, 1994.

[30] K. Ogata and Y. Yang, *Modern control engineering*, vol. 5. Pearson Upper Saddle River, NJ, 2010.

[31] B. C. Kuo, *Automatic control systems*. Prentice Hall PTR, 1987.

[32] T. U. ÖLÇER, *H2/H Mixed Robust Controller Synthesis for a Fin Actuation System*. PhD thesis, Citeseer, 2013.

[33] E. Thöndel, "Linear electromechanical actuator as a replacement of hydraulic cylinder for electric motion platform for use in simulators," *Recent Researches in Applied Informatics*, pp. 290–295, 2011.

[34] P. Yedamale, "Brushless dc (bldc) motor fundamentals," *Microchip Technology Inc*, vol. 20, pp. 3–15, 2003.

[35] A. Hughes and B. Drury, *Electric motors and drives: fundamentals, types and applications*. Newnes, 2019.

[36] W.-H. Hsieh and K.-B. Chang, "Modeling and control of a novel ball screw mechanism," *Journal of Marine Science and Technology*, vol. 22, no. 6, pp. 754–761, 2014.

[37] R. Crowder, *Electric Drives and Electromechanical Systems: Applications and Control*. Butterworth-Heinemann, 2019.

[38] G. S. Tombul, "Real time control of a fin loading system," in *2016 17th International Carpathian Control Conference (ICCC)*, pp. 747–752, IEEE, 2016.

[39] L. Ljung, "State of the art in linear system identification: Time and frequency domain methods," in *Proceedings of the 2004 American Control Conference*, vol. 1, pp. 650–660, IEEE, 2004.

[40] K. J. Keesman, *System identification: an introduction*. Springer Science & Business Media, 2011.

[41] S. Skogestad and I. Postlethwaite, *Multivariable feedback control: analysis and design*, vol. 2. Wiley New York, 2007.